Cell Reports
Medicine

Article

# Checkpoint blockade-related CNS adverse events are characterized by neurotoxic T helper cells with sustained neuroantigen reactivity

## Graphical abstract

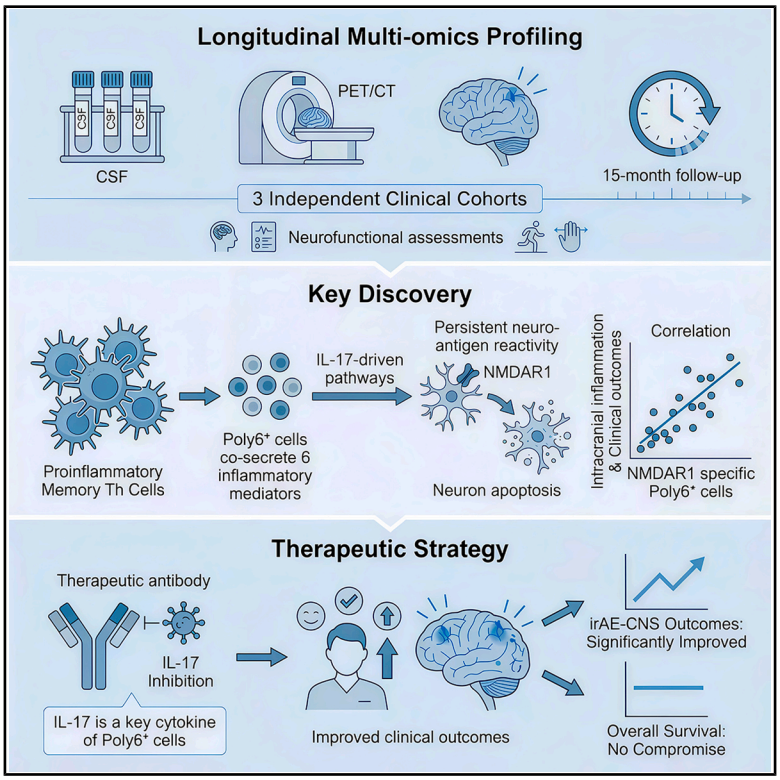


## Highlights

- A distinct poly6+ Th cell population is identified in the CSF of irAE-CNS patients
- Poly6+ Th cells show persistent neuroantigen reactivity and drive neuronal injury
- Poly6+ Th cell abundance correlates with neuroinflammation severity and poor outcomes
- IL-17 blockade mitigates irAE-CNS pathology, offering a targeted therapeutic strategy

## Authors

Yifei Ma, Ao Zhang, Jiacai Lin, ..., Rui Li, Haizhou Liu, Shangeng Weng

## Correspondence

zhonggq@sysucc.org.cn (G.Z.), lirui158@gmail.com (R.L.), liuhaizhou@fjmu.edu.cn (H.L.), shangeng@sina.com (S.W.)

## In brief

Ma et al. identify a unique polyfunctional CD4⁺ T cell subset (poly6+ Th) in irAEs-CNS. These cells persistently react to neuroantigens (e.g., NMDAR1) and drive neuronal injury, and their abundance correlates with severe neuroinflammation and poor outcomes. IL-17 blockade alleviates pathology, suggesting a targeted therapeutic strategy.

Ma et al., 2026, Cell Reports Medicine 7, 102700
April 21, 2026 
https://doi.org/10.1016/j.xcrm.2026.102700

CellPress

Cell Reports Medicine

CellPress
OPEN ACCESS

Article

# Checkpoint blockade-related CNS adverse events are characterized by neurotoxic T helper cells with sustained neuroantigen reactivity

Yifei Ma,[1,2,3,4,33] Ao Zhang,[5,6,33] Jiacai Lin,[7,33] Fadian Ding,[1,2,3,4,33] Xinjia Wang,[8,9] Weidong Wang,[9] Guangmin Jian,[10] Jingyao Zhang,[11] Pengfei Zhu,[10] Yue Ma,[12] Jun Lv,[13] Hongjun Zheng,[14] Jin Li,[15] Tong Wu,[16] Jiling Zeng,[6,17] Yongluo Jiang,[6,17] Yiwei Xu,[18] Xiajie Lyu,[19] Youlong Wang,[20] Yiming Li,[21] Nianqi Liu,[22] Zong-Qing Zheng,[23,24]

*(Author list continued on next page)*

[1]Department of Hepatobiliary and Pancreatic Surgery, the First Affiliated Hospital of Fujian Medical University, Fuzhou, China
[2]Institute of Abdominal Surgery, the First Affiliated Hospital of Fujian Medical University, Fuzhou, China
[3]Fujian Provincial Key Laboratory of Immunotherapy for Cancer, the First Affiliated Hospital of Fujian Medical University, Fuzhou, China
[4]Department of Hepatobiliary and Pancreatic Surgery, National Regional Medical Center Binhai Campus of the First Affiliated Hospital, Fuiian Medical University, Fuzhou, China
[5]Department of Clinical Laboratory, State Key Laboratory of Oncology in South China, Collaborative Innovation Center for Cancer Medicine, Guangdong Key Laboratory of Nasopharyngeal Carcinoma Diagnosis and Therapy, Sun Yat-sen University Cancer Center, Guangzhou, China
[6]State Key Laboratory of Oncology in South China, Guangdong Key Laboratory of Nasopharyngeal Carcinoma Diagnosis and Therapy, Guangdong Provincial Clinical Research Center for Cancer, Sun Yat-sen University Cancer Center, Guangzhou, China
[7]Department of Neurology, Hainan Hospital of Chinese PLA General Hospital, Sanya, China
[8]Department of Orthopedics and Spine Surgery, the Second Affiliated Hospital of Shantou University Medical College, Shantou, China
[9]Department of Orthopedics and Spine Surgery, Cancer Hospital of Shantou University Medical College, Shantou, China
[10]Department of Clinical Laboratory & Key Clinical Laboratory of Henan Province, The First Affiliated Hospital of Zhengzhou University, Zhengzhou, China
[11]Department of Medicine, Nuvance Health Danbury Hospital, Danbury, CT, USA
[12]Department of Laboratory Medicine, Taiyuan Central Hospital of Shanxi Medical University, Taiyuan, China
[13]Department of Infectious Diseases, the First Affiliated Hospital of Zhengzhou University, Zhengzhou, China
[14]XLifeSc, Ltd, Guangzhou, China
[15]Department of Anesthesiology, Shanxi Bethune Hospital, Shanxi Academy of Medical Sciences, Third Hospital of Shanxi Medical University, Tongji Shanxi Hospital, Taiyuan, China
[16]Department of Ophthalmology, Chinese PLA General Hospital Hainan Branch, Sanya, China
[17]Department of Nuclear Medicine, State Key Laboratory of Oncology in South China, Collaborative Innovation Center for Cancer Medicine, Sun Yat-sen University Cancer Center, Guangzhou, China
[18]Department of Clinical Laboratory Medicine, Cancer Hospital of Shantou University Medical College, Shantou, China

*(Affiliations continued on next page)*

## SUMMARY

The immune-related adverse events of central nervous system (irAEs-CNS) are rare yet life-threatening complications arising from immune checkpoint inhibitor therapies, with no effective treatments. The intracranial immune landscape in irAE-CNS remains poorly characterized. Through longitudinal multi-omics profiling of cerebrospinal fluid from three independent clinical cohorts—combined with serial cerebral positron emission tomography/computed tomography (PET/CT) imaging, neurofunctional assessments, and 15-month clinical follow-up, we identify a defined proinflammatory memory T helper cell population specific to irAEs-CNS. These cells co-secrete six signature inflammatory mediators (poly6+ cells) linked to interleukin (IL)-17-driven pathways, exhibit persistent neuroantigen reactivity, and could induce neuron apoptosis. Notably, NMDAR1-specific poly6+ cells are correlated with intracranial inflammation states and clinical outcomes of the disease. Therapeutically, inhibition of IL-17—a key cytokine of poly6+ cells—significantly improves irAE-CNS outcomes without compromising overall survival rates. Our study uncovers neuroantigen-specific proinflammatory Th cells as central drivers of irAE-CNS pathogenesis, offering mechanistic insights and potential therapeutic targets for this debilitating condition.

CellPress
OPEN ACCESS

Cell Reports Medicine
Article

Yu Si Niu,[25] Zhenyun Guo,[1,2,3,4] Ningnan Fang,[9] Wei Jiang,[3,26,27] Lihong Wang,[3,26] Jiahao Chen,[3,26,27] Mengqin Yuan,[3,26,27] Qi Huang,[5,6] Jinjian Li,[28] Jun Lu,[28] Bocen Chen,[29] Tong Huang,[30] Tingting He,[31] Guanqing Zhong,[5,6,*] Rui Li,[32,*] Haizhou Liu,[3,26,27,*] and Shangeng Weng[1,2,3,4,34,*]

[19]Internal Medicine Department, Jacobi Medical Center, 1400 Pelham Play S, Bronx, NY, USA
[20]Department of General Surgery, Hainan Hospital of People's Liberation Army General Hospital, Sanya, China
[21]Department of Neurosurgery, Beijing Tiantan Hospital Capital Medical University, Beijing, China
[22]Faculty of Psychology, Institute of Educational Science, Huazhong University of Science and Technology, Wuhan, China
[23]Department of Neurosurgery, Neurosurgery Research Institute, The First Affiliated Hospital, Fujian Medical University, Fuzhou, China
[24]Department of Neurosurgery, Binhai Branch of National Regional Medical Center, The First Affiliated Hospital, Fujian Medical University, Fuzhou, China
[25]Acute Communicable Disease Epidemiology Division, Dallas County Health and Human Services, Dallas, TX, USA
[26]National Regional Medical Center, Binhai Campus of the First Affiliated Hospital, Fujian Medical University, Fuzhou, China
[27]Department of Bioinformatics, Fujian Key Laboratory of Medical Bioinformatics, School of Medical Technology and Engineering, Fujian Medical University, Fuzhou, China
[28]Department of Hepatobiliary Surgery, the First Affiliated Hospital of Shantou University Medical College, Shantou, China
[29]Key Laboratory of Biochemistry and Molecular Biology, Hainan Medical University, Haikou, China
[30]Department of General Surgery, General Hospital of XinJiang Military Command, Urumqi, China
[31]Department of Thoracic Surgery, The First People's Hospital of Shangqiu City Affiliated to Xinxiang Medical University, Shangqiu, China
[32]Department of Neurology of First Affiliated Hospital, Institute of Neuroscience, Fujian Medical University, Fuzhou, China
[33]These authors contributed equally
[34]Lead contact
*Correspondence: zhonggq@sysucc.org.cn (G.Z.), lirui158@gmail.com (R.L.), liuhaizhou@fjmu.edu.cn (H.L.), shangeng@sina.com (S.W.)
https://doi.org/10.1016/j.xcrm.2026.102700

## INTRODUCTION

Immune checkpoint inhibition (ICI) therapy has significantly prolonged the survival prognosis across nearly all cancer types by activating the tumor immune environment. However, it simultaneously unleashes autoimmune conditions in almost all organs, leading to immune-related adverse events (irAEs) with an incidence ranging from 10% to 90%.[1] Most irAEs occur in barrier sites, such as the skin, colon, and lungs, but rarely in solid organs.[1] Around 1%–3% of irAEs affect the central nervous system ([CNS], irAEs-CNS).[2,3] irAEs-CNS are clinically diverse and can have an unpredictable onset following ICI initiation. Common symptoms include headache, altered mental status, and psychobehavioral changes.[4,5] Although being rare in incidence, anecdotal case series suggest that irAE-CNS is characterized by intracranial inflammation, poor response to anti-inflammatory steroid treatment,[6] and high rates (over 40%) of long-term functional sequelae.[5,6] Few studies have yet explored the patterns of intracranial inflammation in relation to local immunopathological environment, clinical assessment dynamics, and brain imaging.

Studies on non-neurological irAEs, such as colitis, arthritis, and myocarditis, have indicated that $CD8^+$ T cells are the primary effector cells of off-target activation. However, recent findings suggest other immune cells, including T helper cells, play a crucial in driving pathogenesis.[7–11] Despite these insights, research into irAEs within the brain remains elusive due to the lack of animal models and limited access to the affected brain tissue. Few studies have examined protein-secreting patterns at the cellular levels within the local immune environment of irAEs-CNS. A notable feature of irAEs-CNS is the prevalence of disease-related autoantibodies targeting specific neuroantigens, although the significance of these antibodies is still not fully understood.[12] Given that the pathogenesis of irAEs-CNS is hypothesized to have an autoimmune background, similar to paraneoplastic encephalopathy, there is a need for further exploration of antigen-stimulating patterns within the brain to link neuroantigen reactivity with immune cell involvement.[12]

Using multi-omic approaches and three independent irAE-CNS cohorts, we identified a disease-specific population of memory $CD4^+$ T cells ($poly6^+$ Th cells) in the cerebrospinal fluid (CSF) with pro-inflammatory characteristics ($CD137^+IL\text{-}17^+MCP1^+CCL11^+MCP4^+$Granzyme $B^+$). Additionally, we showed that $poly6^+$ Th cells are positively correlated with the clinical severity of the patients with irAEs-CNS, and the functional and clonal phenotype of $poly6^+$ Th cells in the CSF remain stable across follow-up trajectories. We also showed that $poly6^+$ Th cells recognize neuroantigen epitopes, offering insights into the relationship between intracranial adaptive immunity and prevalent antigens in irAEs-CNS. Finally, the blockade of interleukin (IL)-17 in patients with irAEs-CNS significantly improves brain function and reduces brain injury compared to standard treatments. Together, our study draws comprehensive landscape of the inflammation dynamics in irAE-CNS during disease progression, contributing to a better understanding of the off-target cellular immunity involved in immune checkpoint blockade cancer therapy.

## RESULT

### Identification of $poly6^+$ $CD4^+$ T cells as a distinct signature of irAEs-CNS

To comprehensively profile the intracranial inflammatory environment of irAE-CNS patients, we obtained CSF samples of irAE-CNS patients at onset ($n$ = 30) as well as various control groups. Control groups included newly diagnosed CNS infection ([CNSI], $n$ = 24) and autoimmune paraneoplastic encephalopathy (AME, $n$ = 35) patients, as well as non-irAE-CNS patients (NC, $n$ = 24). We examined the inflammatory protein landscape using inflammation-targeted OLINK proteomic panels (406 proteins) in these CSF samples (Figures 1A–1D). We identified and quantified 335 proteins in CSF samples of irAE-CNS and 3 control

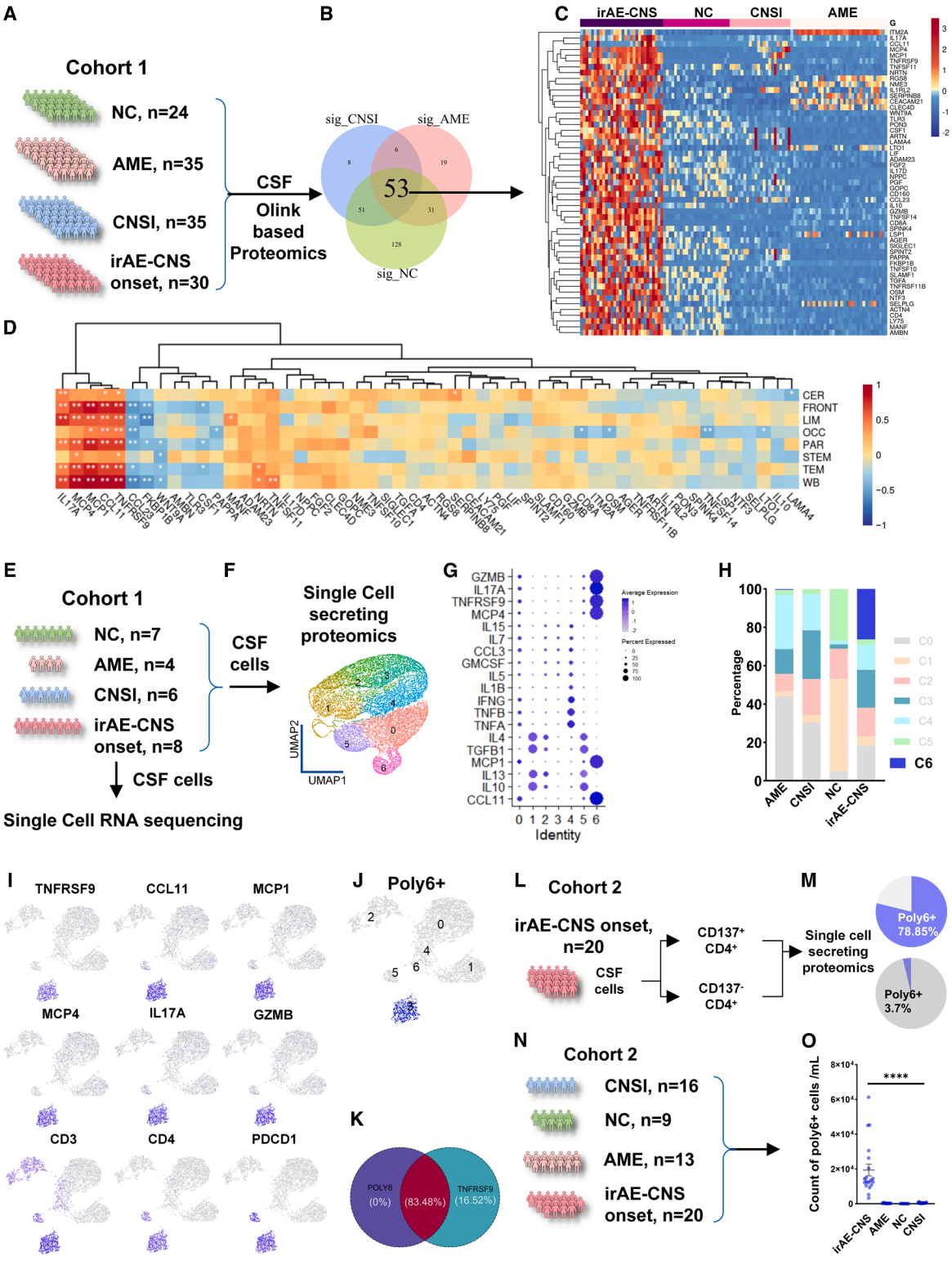


**Figure 1. Identification of poly6+ T helper cells in patients with irAEs-CNS**

(A–C) Proteomic screening of disease-specific CSF proteins (related to demographic data of Table S1). (A) Diagram showing OLINK-based proteomic analysis performed on CSF from irAE-CNS patients at onset ($n$ = 30) as well as 3 control groups (NC, $n$ = 24; CNSI, $n$ = 24; AME, $n$ = 35). (B) Venn diagram showing

*(legend continued on next page)*

groups with 53 proteins showing significant upregulation in the irAE-CNS patients, including TNFα, TNFβ, IFNγ, CCL11, MCP4, MCP1, TNFRSF9, and IL-17A (Figures S1A–S1C; Figures 1A–1C). These results suggest the involvement of inflammation-related proteins in the pathology of irAEs-CNS. Additionally, our previous work suggested that 18-F fluorodeoxyglucose (FDG) positron emission tomography/computed tomography (PET/CT) metabolic signatures could serve as diagnostic biomarkers to monitor irAE-CNS pathologies.[13] Therefore, we performed a correlation analysis between regional 18-F FDG PET/CT metabolic mean standard uptake value (SUVmean) and protein levels at the onset stage (Figure 1D). The SUVmean values of multiple brain regions, particularly the limbic area, temporal lobe, and parietal lobes, were found to have significant correlation with the levels of these proteins (CCL11, MCP4, MCP1, TNFRSF9, and IL-17A, Figure 1D). These results suggest that these proteins could serve as irAE-CNS-specific biomarkers.

Next, we employed single-cell secreting proteomics to identify cell populations responsible for secreting these proteins (Figure 1E). We procured a total of 9,075 cells from irAE-CNS patients at onset ($n$ = 8), 8,687 cells from CNSI patients ($n$ = 6), 7,222 cells from AME patients ($n$ = 4), and 10,728 cells from NC ($n$ = 7, Figures 1E and 1F; Figures S1D and S1E). The uniform manifold approximation and projection (UMAP) plot, generated through dimensionality reduction, grouped all cells into 8 clusters (Figure 1E; Figures S1D and S1E). Six proteins, including TNFRSF9, CCL11, MCP1, MCP4, IL-17A, and Granzyme B, were predominantly found in cluster 6 (Figures 1G and 1H), and, therefore, we named these cells poly6+ cells. This observation suggests that cluster 6 possesses polyfunctional characteristics. These proteins were nearly all identified as irAE-CNS-related biomarkers in prior mixed proteomic analysis (Figure 1D).

We then performed single-cell RNA sequencing on CSF-derived cells from 8 irAE-CNS donors to further characterize phenotypic features for poly6+ cells. A UMAP plot mapped all cells by dimension reduction into 8 clusters (Figures S1F and S1G). All 6 protein genes associated with poly6+ cells were highly expressed in cluster 2 (Figure 1I; Figure S1H), and poly6+ cells were exclusively found in this cluster (Figure 1J). Among the top-expressed genes in cluster 2, TNFRSF9 was predominantly expressed in poly6+ cells (Figure 1K). Notably, 83.48% of *TNFRSF9*+ (gene of CD137) cells were poly6+ cells, and all poly6+ cells were localized within the *TNFRSF9*+ cell population (Figure 1K). Other marker genes highly expressed in cluster 2 included *CD3*, *CD4*, and *PDCD1* (Figure 1I; Figure S1H), indicating that poly6+ cells are T helper cells. This corroborates previous findings that irAEs are characterized by effector T cells.[14] These findings also indicate that poly6+ cells are primarily activated, poly-functional CD4+ T cells in the context of iatrogenic intracranial inflammation, distinguishing their role from that of CD8+T cells in other organs affected by irAEs, such as thyroid,[15] heart,[16] colon,[17] and liver.[18]

Since TNFRSF9 (4-1BB, CD137) is predominantly membrane-bound, we positively sorted CD137+ cells in the second cohort, which included 20 irAE-CNS patients at onset, and performed single-cell secreting proteomics on CD137+ and CD137− $CD4^+$ CSF samples (Figure 1L; Figures S1I and S1J). Our analysis revealed that nearly all poly6+ cells were found in the CD137+ samples (78.85%), with few detected in the CD137- samples (3.7%), confirming that poly6+ cells are CD137+ $CD4^+$ cells (Figure 1M; Figures S1K–S1M). Next, using single-cell membranous proteomics (Figure 1N; Figure S2A), we further confirmed that $CD4^+$ CD137+ PD1+ cells are enriched in patients with irAE-CNS as compared to control groups (NC, $n$ = 9; CNSI, $n$ = 16; and AME, $n$ = 13) (Figure 1O).

We then performed functional annotations of these proteins and found that most of the poly6 proteins were related to IL-17 pathways, suggesting that IL-17A may play a key role in driving the pathogenesis of irAEs-CNS (Figures 2A and 2B). To explore the clinical relevance, we found a strong correlation between the proportion of poly6+ cells and 18-F FDG PET/CT metabolic levels, specifically in the limbic area (Figure 2C). This finding

overlapping proteins after comparison between irAE-CNS and control groups (related to Figures S1A–S1C; Table S1). (C) Heatmap showing levels of highly expressed, irAE-CNS-specific CSF proteins in all sampling groups. sig_CNSI, proteins that are significantly up-regulated in irAEs-CNS as compared to CNSI; sig_NC, proteins that are significantly up-regulated in irAEs-CNS as compared to NC; sig_AME, proteins that are significantly up-regulated in irAEs-CNS as compared to AME (related to Table S1).

(D) Correlative analysis of 18F FDG PET/CT SUVmean values of each segmented brain region and expression levels of proteins found to be highly expressed in irAE-CNS patient samples ($n$ = 30).

(E–H) Single-cell secreting proteomics to identify poly6+ cells. (E) Diagram showing single-cell secreting proteomic analysis and single-cell RNA sequencing analysis in irAE-CNS patients as well as 3 control groups. (F) UMAP clustering defined by single-cell secreting proteomics (total of 35,712 cells) of CSF samples from all patients, including cells from irAE-CNS patients (9,075 cells, $n$ = 8), NC patients (10,728 cells, $n$ = 7), AME patients (7,222 cells, $n$ = 4), and CNSI patients (8,687 cells, $n$ = 6). Groups of patients projected on UMAP plot were shown in Figures S1D and S1E. (G) Signature proteins of each cluster were depicted as the bubble plot based on the above single-cell data. (H) Distribution of cell clusters in each group, showing cluster 6 (C6) was almost exclusively populated in irAE-CNS samples.

(I–K) Single-cell RNA sequencing to identify features of poly6+ cells (using CSF cells from the 8 irAE-CNS donors in F). (I) Genes related to poly6+ cells (TNFRSF9, GZMB, IL17A, CCL11, MCP1, and MCP4) and cellular subtyping (CD3, CD4, and PDCD1) projected on UMAP plot. (J) UMAP clustering to identify poly6+ cells. (K) Venn plot showing numbers of TNFRSF9 gene+ cells and poly6+ cells, exhibiting that all poly6+ cells express TNFRSF9.

(L and M) Validation of poly6+ cell phenotype by sorting. (L) Diagram showing single-cell secreting proteomic testing performed on CD137+ as well as CD137− sorted CSF samples from 20 irAE-CNS patients at onset (cohort 2). (M) Distribution of poly6+ cells in CD137+ and CD137− samples from these 20 patients.

(N and O) Single-cell membranous proteomic validation across cohorts. (N) Diagram showing single-cell membranous proteomic testing in irAE-CNS patients as well as 3 control groups, including samples of irAE-CNS ($n$ = 20, from cohort 2 onset), NC ($n$ = 9), AME ($n$ = 13), and CNSI groups ($n$ = 16, related to demographic data of Table S1). (O) Absolute count of $CD4^+$ CD137+ CD45RA− CCR7− PD-1+ cells (poly6+ phenotype) in patients of each group revealed by single-cell membranous proteomics. sig_NC/AME/CNSI, significantly up-expressed proteins compared to NC/AME/CNSI patient group. Statistical significance for comparisons across multiple groups was determined by one-way ANOVA with Tukey's post hoc test. ****$p < 0.0001$. Data are representative of at least two independent experiments or analyses. Bar graphs show mean ± SEM of n biological replicates as indicated in each panel.

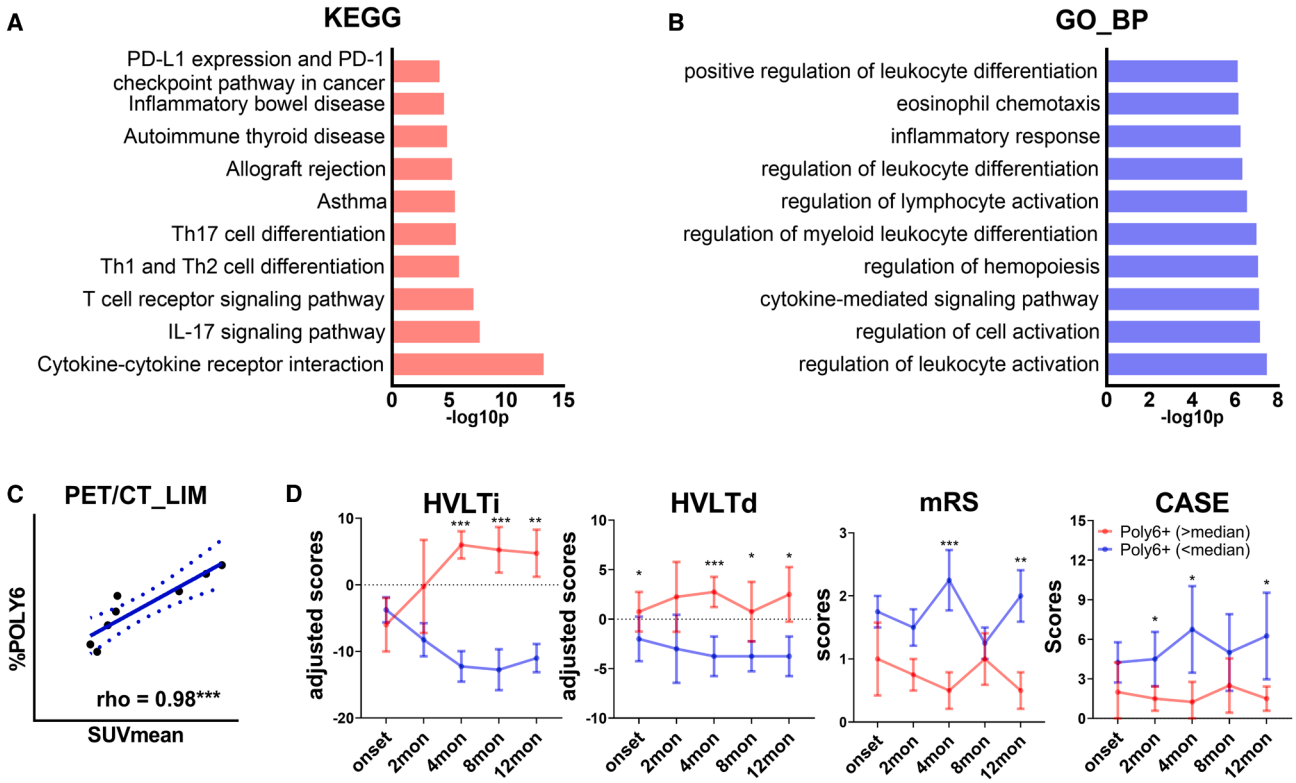


**Figure 2. Pro-inflammatory poly6+ T helper cells are linked with the clinical severity of irAEs-CNS**

(Analyses in this figure are based on data from the 8 irAE-CNS patients in cohort 1, as identified in Figures 1F–1H).

(A and B) Functional annotations of genes of poly6+ cells (identified in Figures 1I and 1K) using Kyoto Encyclopedia of Genes and Genomes (KEGG) (A) and Gene Ontology (GO) (B) databases, suggesting a dominant role of IL-17-related pathway.

(C) Correlation plot of SUVmean values of limbic region PET/CT imaging and the proportion of poly6+ cells determined by single-cell secreting proteomics (Figures 1F–1H) in each irAE-CNS patient in cohort 1 ($n = 8$).

(D) Dynamic changes of BFTs (related to Table S6) scores, including HVLTi, HVLTd, mRS, and CASE, measured at 5 time points in irAE-CNS patients, categorized by high and low median values of poly6+ cell proportions measured at onset in each patient in cohort 1 ($n = 8$). Adjusted scores: follow-up BFT score − onset BFT score. HVLTi, immediate Hopkins Verbal Learning Test-Revised; HVLTd, delayed Hopkins Verbal Learning Test-Revised; mRS, modified Ranking Scale; CASE, Clinical Assessment Scale in Autoimmune Encephalitis; std_SVmean, mean standard uptake value; PET/CT_LIM, limbic area SUVmean of PET/CT.

Statistical significance was determined by unpaired two-tailed Student's $t$ test for comparisons between high- and low-poly6+ groups (D) and by Pearson correlation analysis (C). $^{*}p < 0.05$, $^{**}p < 0.01$, $^{***}p < 0.001$. Data are from $n = 8$ irAE-CNS patients (biological replicates) in cohort 1.

corroborates previous finding that intracranial inflammation of irAEs-CNS was most prominent and prevalent in the limbic area.[3,19] Furthermore, patients with a higher proportion of poly6+ cells showed poorer performance on a 12-month follow-up brain function test (BFT) (Figure 2D), indicating objective cognitive deficits and diminished overall function. Notably, this aligns with our prior cohort study suggesting that checkpoint inhibitor monotherapy may lead to progressive cognitive impairments in treatment-active lung cancer patients.[20] Together, these data collectively suggest poly6+ cells could serve as a disease-specific marker in irAE-CNS patients both before and after anti-inflammatory treatment.

## The surface, functional, and clonal phenotypes of CD137+ T helper cells are stable in patients with irAEs-CNS

We then investigated the dynamics of phenotypes and clonotypes of CSF-derived CD137+ cells during long-term follow-up and sequential sampling (Figure 3A). At 2 time points in cohort 1 (onset and 3 months), we compared the poly6+ secreting patterns of CD137+ cells and found stable secretion patterns from onset (68.26%) to the 3-month stage (83.45%, Figure 3B; Figure S2B). When standardized by patient sampling, all patients exhibited consistent contributions of poly6+ cells at both sampling points (Figure 3C). This finding was further validated in cohort 2 (Figure 3D), where all 6 proteins exhibited similarly high levels in CD137+ cells across 3 sampling time points (Figure 3E). Taken together, these results confirm that the polysecreting ability of CD137+ cells remains persistent throughout follow-up.

Next, we investigated the single-cell membranous proteomic characteristics of CD137+ cells at 3 time points in cohort 2 (Figure 3F; Figure S2C). We found that the CD137+ T helper cells were stable from onset to 12-month stage (Figure 3G; Figures S2C and S2D). Results from fluorescence-activated cell sorting at all stages also supported this finding (Figures S2E–S2I). Together, these results indicate that CD137+ cells maintain a stable and

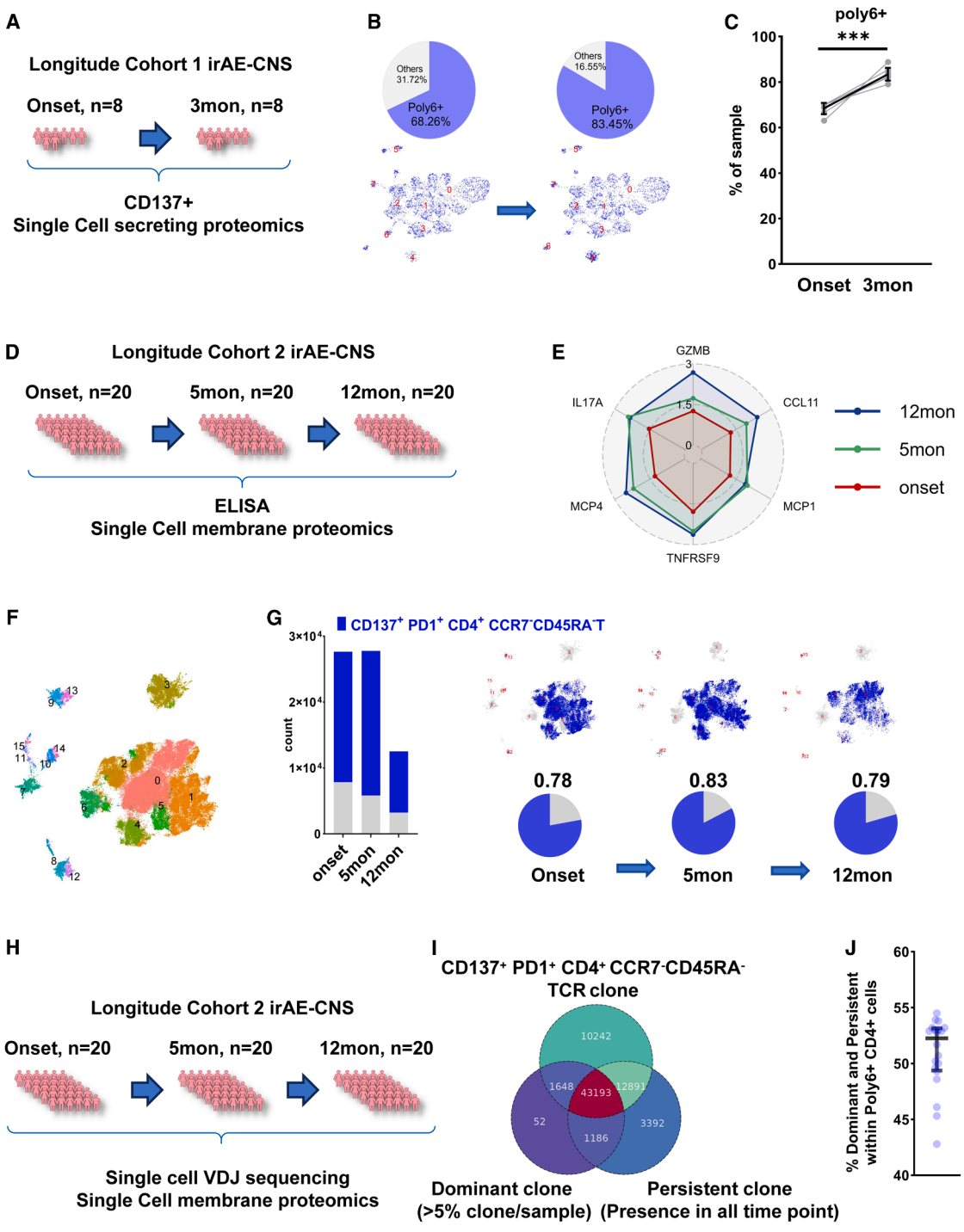


**Figure 3. The surface, functional, and clonal phenotypes of poly6+ T cells are stable in patients with irAEs-CNS**

(This figure contains longitudinal analyses from two independent cohorts: A–C from cohort 1, and D–J from cohort 2.).

(A–C) Single-cell secreting proteomic analysis on CD137+ cells of two-time point sampling in cohort 1 (the same 8 irAE-CNS patients as in Figures 1F–1H and 2). (A) Sampling and experiment diagram illustrating longitudinal assessment at onset and the 3-month follow-up. (B) Proportions of poly6+ cells at onset and 3-month stages as visualized in pie chart and UMAP plot. (C) Proportions of poly6+ cells in each patient across both time points.

(D–J) Comprehensive longitudinal phenotyping and clonal analysis in cohort 2. (D) Sampling and experiment diagram showing ELISA study and single-cell membranous proteomics of CD137+ Th cells from 20 irAE-CNS patients in cohort 2 at three time points (onset, 5 months, and 12 months). (E) Signature proteins of poly6+ cells were measured by ELISA using samples from onset, 5-month, and 12-month stages of 20 patients, depicted as log2Fc of cytokine levels in cell culture media of CD137+ cells over CD137− cells in each time point. (F) UMAP clustering defined by single-cell membrane proteomics of CD137+ cells of 20

*(legend continued on next page)*

robust surface and functional phenotype throughout follow-up in the CSF of irAE-CNS patients.

To address the functional relevance of poly6+ cells, we conducted proof-of-concept experiments to evaluate their neurotoxic potential (Figures S2J–S2M). Using an *in vitro* co-culture system with human neuronal cell lines (SH-SY5Y), we demonstrated that poly6+ cells induce significant neuronal apoptosis, as quantified by using Annexin V/7AAD staining. This cytotoxicity was modulated via IL-17 secretion. We show that IL-17A antagonist suppressed neuronal death, thus linking poly6+ cells to neurotoxicity.

The observation of a stable phenotype in CD137+ cells throughout follow-up supports the hypothesis that certain clonotypes may act as persistent drivers of intracranial inflammation.[21] To explore this, we analyzed the paired single-cell VDJ repertoire in CD137+ cells at three time points to investigate the dynamics of CD137+ cells in irAE-CNS patients in cohort 2 (Figure 3H). Cross-matching clonotypes across the three sampling time points revealed persistent clonotypes (i.e., clonotypes that were fully matched at all three time points in CD137+ cells), and any clonotype with >5% frequency per sample was defined as dominant. These clonotypes may provide critical insights into the effector mechanisms driving intracranial inflammation in irAEs-CNS. In total, 60,662 cell clones were identified as persistent clones and 46,079 clones were found as dominant clones across all time points. We then matched these clones with cells expressing PD1+CD137+CD4+CCR7−CD45RA− T cells to explore the relationship between clonotypes with phenotypes. A significant association was found among persistent cells, dominant cells, and PD1+CD137+CD4+CCR7−CD45RA− T cells (Figure 3I). This finding suggests clonal activation in CD137+ cells is persistent, while non-clonal activation is generally temporary. Our data demonstrate that persistent clonal expansion mainly happened in PD1+CD137+CD4+CCR7−CD45RA− phenotype of CD137+ T cells (Figure 3J). Together, we conclude that PD1+CD137+CD4+CCR7−CD45RA− T cells were persistently and robustly activated in CD137+ cells. Given the autoimmune hypothesis of irAE-CNS pathology and previous reports of therapeutic resistance, our findings suggest that potential antigenic stimuli are likely driving the sustained and robust activation of poly6+ cells.

## Poly6+ T cells in the CSF of irAE-CNS patients recognize CNS antigens

The presentation of irAE is usually organ-specific. Emerging evidence suggests that irAE-CNS may be a specific form of irAE potentially driven by intracranial neuroantigens that may serve as pervasive autoimmune stimuli to checkpoint-blocked T cells.[22,23] Supporting this hypothesis, autoantibodies targeting these antigens have been identified in case series.[22,24] As such, one of the key elements of irAE-CNS pathogenesis relies in the interaction between disease-specific adaptive immunity and their response to prevalent neuroantigens.[3] To explore the antigen specificity of poly6+ T cells, we tested a serum panel of CNS-related auto-antibodies that are involved in driving autoimmune encephalopathies in 3 independent cohorts (Figures S3A–S3C). We found 5 autoantibodies with high proportions of positivity, including NMDAR1, SOX1, DPYSL5, ELAVL4, and GRIA1 (Figures S3A–S3C). To further investigate the relationship between immune cells and antigens in CSF, we sorted antigen-specific CSF cells using 15-mer peptide-major histocompatibility complexes (MHCs) derived from 415 overlapping peptide pools (OPPs). We then sequenced the neuroantigen-reactive VDJ repertoire of these cells specific to these OPPs in 2 time points within the cohort 2 (Figure 4A; Figures S4Aand S4B). Additionally, we explored clonotype associations with CD137+ VDJ repertoire in paired sample data.

Following quality control, we identified 5,014 and 3,488 antigen-reactive cell clones at onset and 5-month time point, respectively. Overall, NMDAR1-reactive cells accounted for the highest proportions of reactive cell clones at both time points (53.5% and 63.5%, respectively, Figure 4B). Additionally, NMDAR1 was the most frequently found antigen in these patients at both stages of sampling (14 and 16 patients, respectively, Figure 4B). The number of TCRαβ clonotypes reactive to NMDAR1 was also the highest among the five tested antigens at both time points (Figures S4C and S4D). To further investigate the relationship between antigen-reactive cells and CD137+ cells, we cross-matched antigen reactive clonotypes with CD137+ TCRαβ clonotypes. We observed that approximately 75% of the sorted cells consistently exhibited a CD137+ PD1+ effector memory phenotype at both stages (Figure 4C). Among these sorted cells, NMDAR1-reactive clones represented the highest proportion at both sampling time points (Figure 4D). Furthermore, within the NMDAR1-reactive cell population, clones specific to the EERITGINDPRLRNP epitope accounted for the largest proportion at both stages (Figure 4E).

Given CD137+ cells carried robust poly6+ phenotype, we next tested whether NMDAR1-reactive T helper cells could also harbor poly6+ functional phenotype by using single-cell secreting proteomics (see gating strategy in Figure S5A). We observed that 70.19% of NMDAR1-reactive T helper cells are poly6 positive (Figures 4F and 4G; Figures S5B and S5C). Furthermore, the proportion of poly6+ cells (per patient) is positively correlated with patients' SUVmean values of multiple brain areas (Figure S5D).

To further validate the surface phenotype and epitope-clonotype binding of NMDAR1-reactive cells, we employed single-cell

irAE-CNS patients at 3 time points (onset, 5 months, 12 months), 9 NC patients (ICI-treated cancer patients without irAEs-CNS), 13 AME patients (paraneoplastic autoimmune encephalopathy), and 16 CNSI patients (CNS infection in cancer patients). Control groups are as described in STAR Methods. (G) Overall cell count and proportions of PD1+ $CD4^+$ CCR7− CD45RA− T cells within the CD137+ sorted population in onset, 5-month, and 12-month samples, visualized in pie chart and UMAP plots. (H) Single-cell VDJ sequencing analysis in onset, 5-month, and 12-month CD137+ Th samples of irAE-CNS patients of cohort 2 (related to demographic data of Table S2). (I) Venn diagram showing the overlap between PD1+ $CD4^+$ CCR7− CD45RA− T cells, persistent cell clones, and dominant cell clones in single-cell membranous proteomics paired with VDJ testing of CD137+ cells of all 3 time points. (J) Dominant and persistent poly6+ cell proportions of each patient sample from cohort 2. Longitudinal data represent biological replicates from two independent cohorts (cohort 1, $n = 8$; cohort 2, $n = 20$) across indicated time points.

Statistical significance for comparisons between groups was determined by unpaired two-tailed Student's $t$ test. $^{***}p < 0.001$.

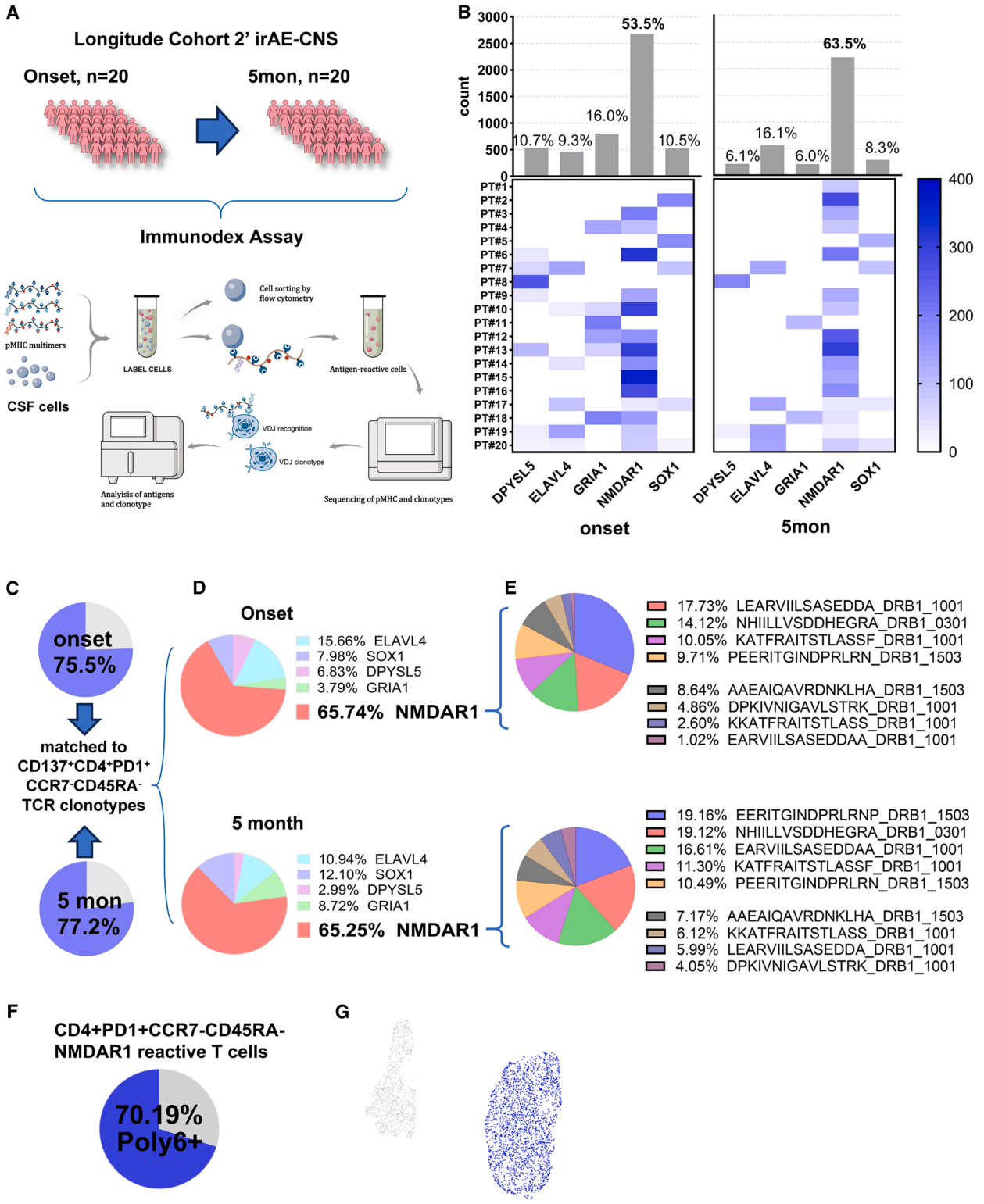


**Figure 4. Poly6+ T cells in the CSF of irAE-CNS patients recognize CNS antigens**

(All analyses in this figure are based on antigen-reactive T cells sorted from the CSF of the 20 irAE-CNS patients in cohort 2 at the indicated time points.)

(A) Diagram of antigen-reactive cell VDJ clonotype finding and analysis workflow using overlapping peptide pool corresponding to 5 neuroantigens (NMDAR1, SOX1, DPYSL5, ELAVL4, and GRIA1) in onset and 5-month samples of irAE-CNS patients in cohort 2 (related to demographic data of Table S2).

*(legend continued on next page)*

membranous proteomics paired with VDJ sequencing on sorted CD137+ NMDAR1-reactive T cells from an independent cohort of irAEs-CNS (cohort 3, demographics in Table S3; Figure 5A). We confirmed that NMDAR1-reactive T cells harbor activated effector memory phenotype (Figures S6A and S6B). Persistently dominant cell clones were mostly enriched in CD137+ NMDAR1-reactive cells (Figure 5B). Also, we found that among all epitopes with epitope-binding persistence (Figure 5C), 5 were the same epitopes found in cohort 2 (Figure 5D) and the most predominant 15-mer peptide accounted for 21.13% (PEERITGINDPRLRN, Figure 5D), thus validating that these 5 epitopes may have durable antigen-presenting abilities throughout follow-up.

We found that patients harboring CD137+NMDAR1+ cells had higher levels of SUVmean values in multiple brain areas and had poorer performance at BFTs (Figures 5E–5G). Correlation analysis suggested that there was significant correlation between intracranial inflammation state and CD4+PD1+ TEM phenotype proportion, as indicated by SUVmean value changes of regional 18-F FDG PET/CT brain imaging and serial BFTs during follow-up (Figure 5H). In conclusion, our data suggest that intracranial NMDAR1-reactive poly6+ cells, which were robustly expanding, correlated with high intracranial inflammation state and poor prognosis.

### Anti-IL-17A treatment improves clinical outcomes of irAEs-CNS in a real-world cohort

The data above suggested that poly6+ Th cells are the major source of IL-17 in the CNS during irAE-CNS. It is known that IL-17 is involved in the pathogenesis of many autoimmune diseases and the blockade of IL-17 has been used to treat autoimmune diseases such as inflammatory arthrophathy[25,26]; yet, the clinical effects of IL-17 blockade on inflammatory CNS diseases remain unknown, and next, we sought to evaluate the clinical efficacy of IL-17-blocking agents for irAEs-CNS in clinical settings. In an observational, multi-center, match-controlled real-world cohort of irAE-CNS patients, we enrolled a total of 50 patients with irAEs-CNS from 3 centers, of whom 17 patients were treated with anti-IL-17A agents (ixekizumab and secukinumab), while 17 were matched via propensity score matching with the other 33 patients who received standard care (Figure 6A, see Figure S7 for comparable baseline characteristics of 1:1 patient pairs; see Tables S4 and S5 for demographic details before and after statistical matching). We followed these patients for 12 months and conducted serial BFTs as well as 18-F FDG PET/CT brain imaging studies on these patients to monitor their disease activity. Patients were given BFTs at 5 sessions during follow-up, including treatment initiation/disease onset and 2-month, 4-month, 8-month, as well as 12-month sessions (Figures S8A–S8D; Figure 6B), and 2-session PET/CT imaging studies (onset and 7-month session, Figure 6C). Our findings revealed significant improvements in SUVmean across all brain regions except the brainstem, as assessed by PET/CT imaging, as indicated by paired Student's t test from onset to final follow-up (Figure 6C). Similarly, all four BFTs demonstrated significant improvement from baseline to the 12-month follow-up (Figure 6B). Also, the improvement level (Δ, defined as the level between the final follow-up and before-treatment assessment) was significantly higher in the anti-IL-17A treatment group in both PET/CT imaging and BFTs (Figures 6B and 6C). Importantly, no significant differences were observed in cancer-related or all-cause mortality rates between the treatment and control groups until final follow-up of cancer-related outcomes (Figures S8E and S8F). These results suggest that anti-IL-17A therapy may significantly improve disease-related outcomes in irAE-CNS patients without impacting all-cause mortality rates.

## DISCUSSION

The underlying mechanisms of irAE-CNS remain elusive. Our study identified a disease-specific poly6+ $CD4^+$ T cell population exhibiting persistent and robust neuroantigen reactivity, which correlated with intracranial inflammation levels throughout disease trajectories. NMDAR1 is predominant autoantigen recognized by poly6+ Th cells and is clonally expanded in the CSF of irAE-CNS patients. Furthermore, we observed that targeting IL-17, a proinflammatory signature cytokine of poly6+ Th cells, could ameliorate irAEs-CNS. This study thus provides direct evidence of intracranial pathological characteristics of irAEs-CNS at cellular, imaging, and clinical levels, offering insight into antigen exposure and immune patterns of autoimmune irAEs in the CNS.[27]

Our work highlights immune mechanisms driven by neuroantigen-reactive T cells and their effector protein signatures, which were linked to intracranial inflammation states represented with imaging and clinical assessments. Importantly, we examined the relationship between T cell repertoire expansion and neuroantigen epitopes during mid- to long-term follow-up, demonstrating adaptive evolution against these epitopes as disease progressed.[28–30] Although autoantigen-immune cell interaction are characterized in other autoimmune disorders, few studies have explored these dynamics in irAEs or irAEs-CNS.[21,28,31] Notably, while irAEs in non-CNS organs are driven by interferon-secreting $CD8^+$ cells, our findings suggested that poly6+ $CD4^+$ T cells maybe the driver of the irAEs-CNS, highlighting the fundamental differences underlying the mechanisms between irAEs-CNS vs. irAEs-non-CNS. Further studies are

(B) Antigen-reactive cell count, sorted with peptide-MHC multimer pools specific to the 5 neuroantigens, from 5 tested neuroantigens in each CSF sample of 20 patients at onset stage of cohort 2, with bar plot showing overall sorted cell count associated with each antigen.
(C) Pie chart showing proportions of antigen-reactive cells (identified in B) matched to CD137+CD4+PD1+CCR7−CD45RA− TCR clonotype defined in the paired single-cell VDJ repertoire analysis (related to Figure 3H).
(D) Pie chart showing proportions of each antigen type in the matched cell pool from (C), with bold item showing the largest reactive type being NMDAR1.
(E) Pie chart showing proportions of each 15-mer peptide-MHC type within the NMDAR1 peptide pool that was recognized by the matched clones.
(F and G) Validation of polyfunctionality in antigen-specific cells. (F) Single-cell secreting proteomic analysis identifying poly6+ cell proportions in sorted CD4+PD1+CCR7-CD45RA− NMDAR1-reactive T cells (gating strategy detailed in Figure S5A). (G) Visualization of the cells analyzed in (F) in UMAP plot. Antigen reactivity data are derived from $n = 20$ biological replicates (cohort 2).

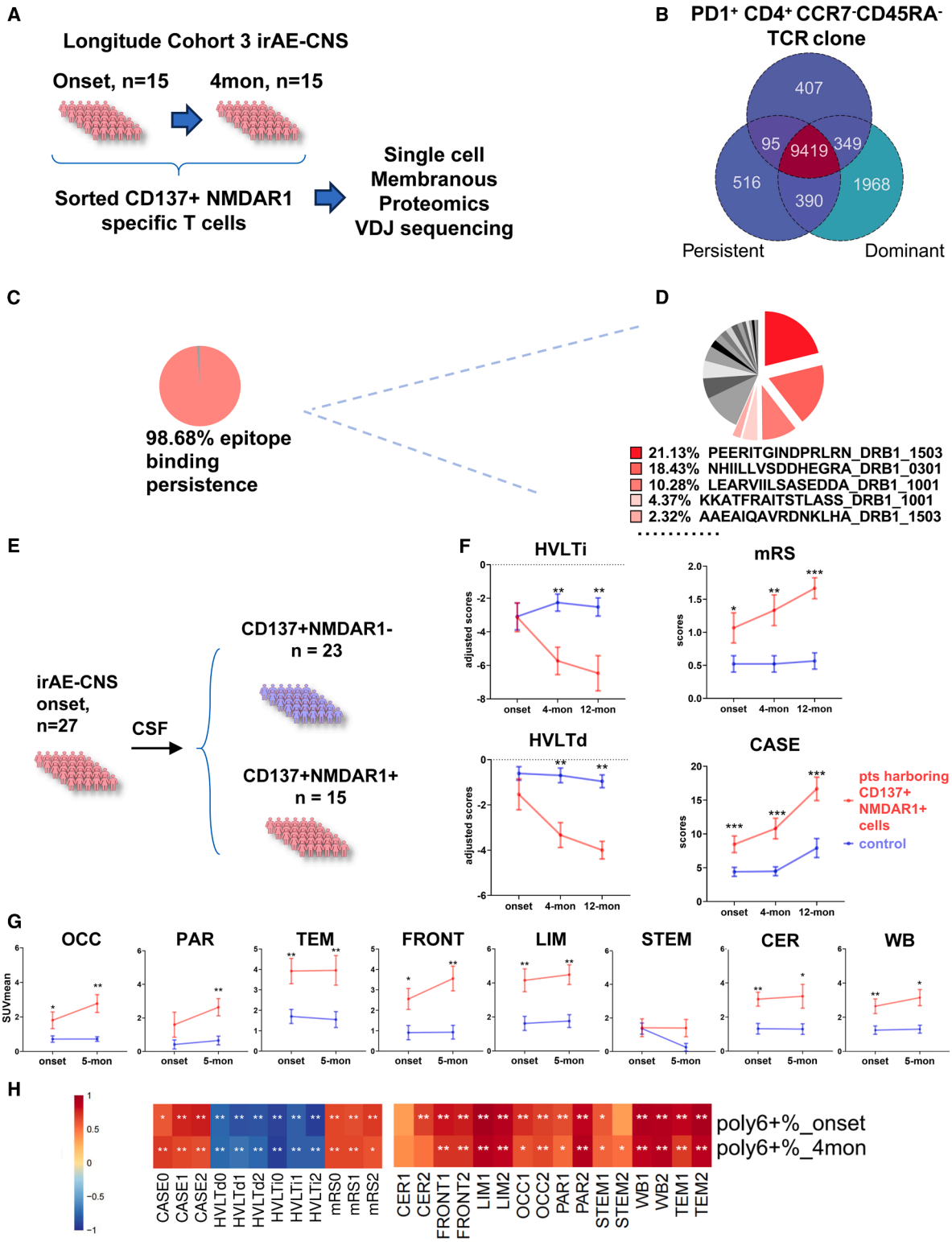


**Figure 5. Validation of NMDAR1 reactivity for poly6+ cells in CSF and clinico-radiological correlates in cohort 3**

(This figure is based on cohort 3, which comprised 38 irAE-CNS patients. Single-cell analyses (B–D) focus on the 15 patients with detectable NMDAR1-specific CD137+ cells, while clinico-radiological analyses (F and G) include all 38 patients stratified by NMDAR1 specificity.)

*(legend continued on next page)*

encouraged to unravel the molecular mechanisms of these polyfunctional protein-secreting patterns.

Our data suggest that poly6+ Th cells serve as the primary source of IL-17 in the CNS during irAE-CNS. This aligns with prior evidence identifying IL-17A as a pathogenic biomarker in autoimmune encephalitis. Preclinical studies have demonstrated that intracranial IL-17A administration could directly induce encephalitis, suggesting the critical role of IL-17A in CNS inflammation.[32–34] The blockade of IL-17 has also been used to treat autoimmune diseases such as inflammatory arthropathies.[25,26] In our multicenter, match-controlled real-world cohort of irAE-CNS patients, we observed that anti-IL-17A therapy significantly improved brain function compared to the standard care, further suggesting the pathogenic role of IL-17A in irAEs-CNS. These findings highlight the need for a randomized controlled trial to establish definitive clinical evidence for IL-17A blockade in irAE-CNS management.

In conclusion, this work establishes poly6+ $CD4^+$ T cells and IL-17A as key factors in irAE-CNS, offering a roadmap for targeted therapies and mechanistic research to address this understudied autoimmune side effect of checkpoint inhibitors.

## Limitations of the study

As the study to characterize immune cell dynamics in intracranial inflammation associated with irAE-CNS, our work has limitations that warrant caution. First, while our study established four independent cohorts of irAEs-CNS—representing the largest investigation of its kind to date, the sample size within each cohort remained relatively small, potentially limiting statistical power, particularly in correlational analyses. Additionally, CSF cell counts remained relatively low, which is attributable to biological constraints, clinical sampling challenges, and cell loss during single-cell protocols-constrained resolution. Using CSF cells cannot fully replicate what is actually occurring in inflamed brain tissue, and future studies of brain tissue samples are encouraged. Our antigen panel was limited to 5 candidates,[23] and the use of wild-type 15-mer peptide multimers (predicted via online databases) may not fully replicate native antigen presentation involving complex structural epitopes.[35] Future studies should explore variable peptide lengths and peptide mutation screens to identify patient-specific neoantigens and T cell receptors (TCRs).[36] Finally, we only adopted MHC class II for multimer construction based upon our single-cell data finding and antigen screening, and thus potential antigens reacting with MHC class I were not evaluated.

## RESOURCE AVAILABILITY

### Lead contact

Further information and requests for resources and reagents should be directed to and will be fulfilled by the lead contact, Shangeng Weng (shangeng@sina.com).

### Materials availability

This study did not generate new unique reagents.

### Data and code availability

- Raw and processed sequencing data are publicly available at the GSA-Human (Genome Sequence Archive for Human) at China's National Genomics Data Center under accession number HRA016812. The proteomics data are available in the PRoteomics IDEntifications Database (PRIDE) under accession number PAD000030. Sharing of raw RNA sequencing data was not allowed by the informed consent signed by patients enrolled in this study. Imaging data reported in this paper will be shared by the lead contact upon request. Any additional information required to reanalyze the data reported in this paper is available from the lead contact upon request.
- This paper does not report any original/custom computer code. All analyses were performed using commercially available software and standard, published pipelines, as detailed in the method details section and listed in the key resources table.
- Any additional information required to reanalyze the data reported in this work paper is available from the lead contact upon request.

## ACKNOWLEDGMENTS

The authors would like to acknowledge the volunteers who participated in the study. Funding: This work was supported by the National Natural Science Foundation of China General Fund Project (82370521 to S.W. and 32370962 to R.L.), National Natural Science Foundation of China Youth Science Fund Project (82102687 to Yifei Ma, 81902470 to J.Lv, 82201922 to A.Z., 62501158 to H.L.), and Regional Joint Key Support Project of National Natural Science Foundation of China (U23A20428 to R.L.). This work was also supported by the Natural Science Foundation of Fujian Province of China (2024J08164 to H.L. and 2025J01753 to Yifei Ma), Fujian Provincial Health and Wellness Science and Technology Plan Project (2024QNA036 to H.L.), and Joint Funds for the Innovation of Science and Technology, Fujian Province (2024Y9121 to H.L., 2023Y9054 to Yifei Ma). (Note: All the funders had no role in the design and conduct of the study.) Ethics approval and consent to participate: The study was approved for retrospective protocol by the institutional review boards of the Affiliated Cancer Hospital of Shantou University Medical College. All procedures was performed according to the Helsinki Declaration (approval no.ST-ZLY-2020-716). Consent for

(A) Research diagram of cohort 3 (related to demographic data of Table S3). Single-cell membrane proteomics and single-cell TCR repertoire of 15 patients with NMDAR1-specific CD137+ cells were performed using sample collected from onset and 4-month follow-up time points.

(B–D) Single-cell analysis of NMDAR1-specific cells. (B) Venn diagram showing number of PD1+ $CD4^+$ CCR7−CD45RA− T cells defined by membrane proteomics, persistent cell clones, and dominant cell clones identified by paired TCR repertoire analysis of both sampling time points. (C) Proportions of cells with epitope binding persistence in both sampling time points among the NMDAR1-specific cells. (D) Proportions of peptides with epitope binding persistence, where non-gray colors show the same peptides found in cohort 2 and gray colors represent peptides not persistently bound.

(E) Stratification schematic. Grouping of CD137+ cells based upon NMDAR1 specificity (related to demographic data of Table S3) for the subsequent analyses in (F and G).

(F and G) Association of NMDAR1 specificity with clinical outcomes in the full cohort 3 ($n$ = 38). (F) Patient scores of brain function tests assessed from onset to 12-month follow-up, divided by patients with and without NMDAR1-specific clones in CD137+ sorted cells. (G) SUVmean values of each segmented brain region in 18F-FDG PET/CT brain imaging during follow-up, divided by patients with and without NMDAR1-specific clones in CD137+ sorted cells.

(H) Correlation heatmaps between proportions of poly6+ cells and BFTs as well as PET/CT brain imaging at two follow-up timepoints.

Statistical significance for comparisons between groups was determined by unpaired two-tailed Student's $t$ test. $^*p < 0.05$, $^{**}p < 0.01$, $^{***}p < 0.001$. Single-cell data are from $n$ = 15 biological replicates, and clinico-radiological data include $n$ = 38 biological replicates.

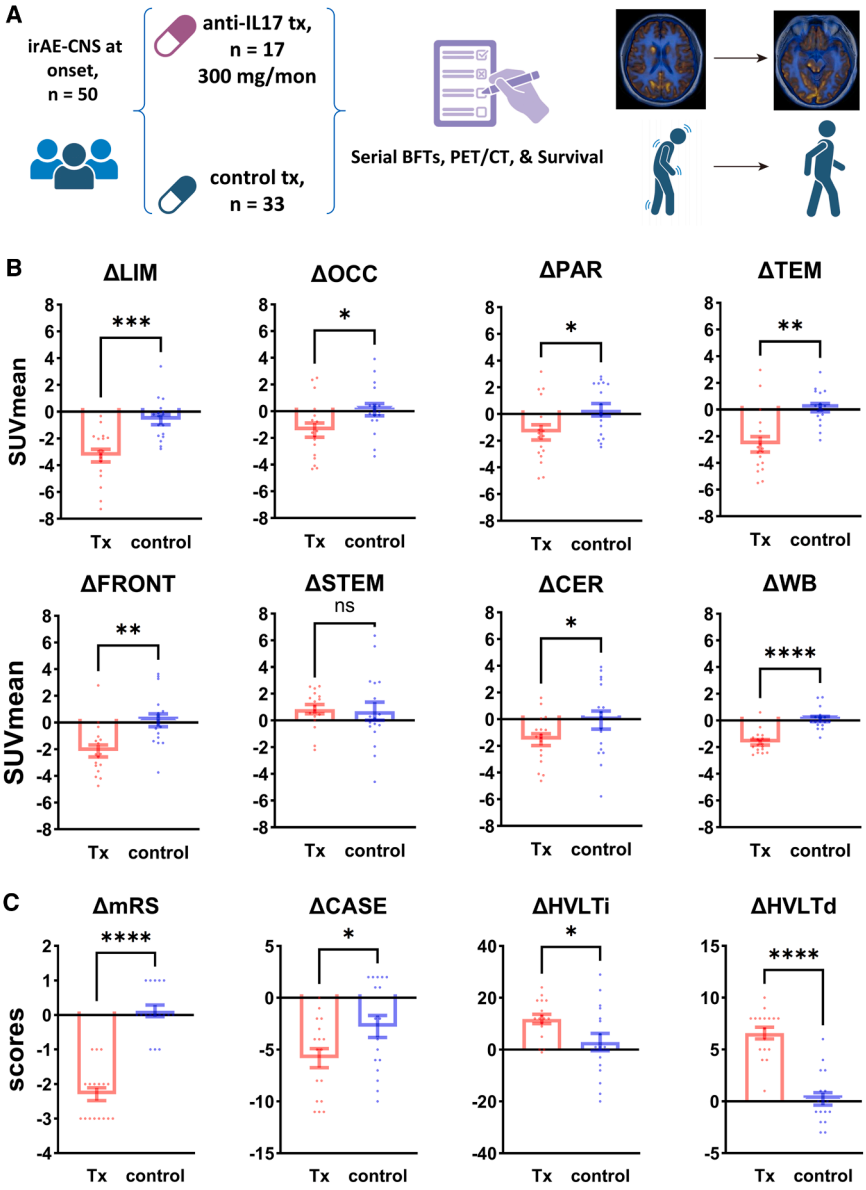


**Figure 6. Treatment with anti-IL-17 improves clinical outcomes in irAE-CNS patients**

(Analysis based on cohort 4. A total of 50 irAE-CNS patients were enrolled, from which 17 received anti-IL-17A agents (Tx group). A propensity-score-matched control group ($n = 17$) was selected from the remaining 33 patients receiving standard care alone.)

(A) Research flowchart of anti-IL-17 treatment as compared to standard-practice control group (see demographic data in supplementary tables) illustrating patient enrollment, treatment allocation, and outcome assessment timeline.

(B) Imaging outcomes. SUVmean value changes of each segmented brain region in 18F-FDG PET/CT brain imaging from onset to the 7-month assessment in anti-IL-17 treatment group and standard-care group (related to demographic data of Table S4). Δ defined as level between 7-month assessment and onset. Statistical comparison was performed using paired Student's *t* test.

(C) Functional outcomes. Brain function test score changes, including HVLTi, HVLTd, mRS, and CASE, from onset to the 12-month assessment in anti-IL-17 treatment group and standard-care group. Δ defined as level between 12-month assessment and onset. Abbreviation: Tx: anti-IL-17 treatment group treated with IL-17A inhibitors (ixekizumab or secukinumab), in addition to standard care as clinically indicated.

Statistical significance was determined by paired two-tailed Student's *t* test for Δ values within each group and unpaired two-tailed Student's *t* test for comparisons between the anti-IL-17A treatment group and the standard-care control group. $^{*}p < 0.05$, $^{**}p < 0.01$, $^{***}p < 0.001$, $^{****}p < 0.0001$. Treatment outcomes are compared between two matched groups of $n = 17$ biological replicates each.

publication: Participants had given written informed consent to the usage of clinical information for medical research.

## AUTHOR CONTRIBUTIONS

S.W., H.L., R.L., and G.Z conceptualized and designed the study and reviewed and revised the manuscript. Yifei Ma, F.D., X.W., W.W., Y.X., X.L., and N.L. designed the data collection instruments, carried out the initial analyses, and wrote the first draft of the manuscript. A.Z., G.J., J.Zhang, P.Z., Yue Ma, H.Z., Y.W., Y.L., W.J., L.W., J.C., M.Y., and D.Z. coordinated and supervised data collection and critically reviewed the manuscript for important intellectual content. J. Lv, J. Lin, Jin Li, T.W., J.Zeng, Y.J., Z.-Q.Z., Y.S.N., Z.G., N.F., Q.H., Jinjian Li, J. Lu, B.C., T. Huang, and T. He collected data and reviewed and revised the manuscript. All authors approved the final manuscript as submitted and agreed to be accountable for all aspects of the work. The work reported in the paper has been performed by the authors unless specified in the text.

## DECLARATION OF INTERESTS

The authors have declared no conflicts of interest.

## STAR★METHODS

Detailed methods are provided in the online version of this paper and include the following:

- KEY RESOURCES TABLE
- EXPERIMENTAL MODEL AND STUDY PARTICIPANT DETAILS
  - Human subjects and clinical cohorts
  - Four independent clinical cohorts were enrolled
  - Summary of participant demographics
  - Diagnostic criteria for irAE-CNS and control groups
  - Key exclusion criteria for all participants included
  - Experimental model: Cell line

## SUPPLEMENTAL INFORMATION

Supplemental information can be found online at https://doi.org/10.1016/j.xcrm.2026.102700.

Received: July 9, 2025
Revised: December 8, 2025
Accepted: February 24, 2026
Published: April 21, 2026

## REFERENCES


1. Fletcher, K., and Johnson, D.B. (2024). Chronic immune-related adverse events arising from immune checkpoint inhibitors: an update. J. Immunother. Cancer *12*, e008591. https://doi.org/10.1136/jitc-2023-008591.
2. Rossi, S., Gelsomino, F., Rinaldi, R., Muccioli, L., Comito, F., Di Federico, A., De Giglio, A., Lamberti, G., Andrini, E., Mollica, V., et al. (2023). Peripheral nervous system adverse events associated with immune checkpoint inhibitors. J. Neurol. *270*, 2975–2986. https://doi.org/10.1007/s00415-023-11625-1.
3. Farina, A., Villagrán-García, M., Vogrig, A., and Joubert, B. (2024). Central nervous system adverse events of immune checkpoint inhibitors. Curr. Opin. Neurol. *37*, 345–352. https://doi.org/10.1097/wco.0000000000001259.
4. Aboseif, A., Vorasoot, N., Pinto, M.V., Guo, Y., Hasan, S., Zekeridou, A., Chen, J.J., and Dubey, D. (2024). Immune Checkpoint Inhibitor-Associated Kelch-Like Protein-11 IgG Brainstem Encephalitis. Neurol. Neuroimmunol. Neuroinflamm. *11*, e200218. https://doi.org/10.1212/nxi.0000000000200218.
5. Pepys, J., Stoff, R., Ramon-Gonen, R., Ben-Betzalel, G., Grynberg, S., Frommer, R.S., Schachter, J., Asher, N., Taliansky, A., Nikitin, V., et al. (2023). Incidence and Outcome of Neurologic Immune-Related Adverse Events Associated With Immune Checkpoint Inhibitors in Patients With Melanoma. Neurology *101*, e2472–e2482. https://doi.org/10.1212/wnl.0000000000207632.
6. Vogrig, A., Muñiz-Castrillo, S., Farina, A., Honnorat, J., and Joubert, B. (2022). How to diagnose and manage neurological toxicities of immune checkpoint inhibitors: an update. J. Neurol. *269*, 1701–1714. https://doi.org/10.1007/s00415-021-10870-6.
7. Wang, R., Singaraju, A., Marks, K.E., Shakib, L., Dunlap, G., Adejoorin, I., Greisen, S.R., Chen, L., Tirpack, A.K., Aude, C., et al. (2023). Clonally expanded CD38 cytotoxic CD8 T cells define the T cell infiltrate in checkpoint inhibitor-associated arthritis. Sci. Immunol. *8*, eadd1591. https://doi.org/10.1126/sciimmunol.add1591.
8. Lechner, M.G., Zhou, Z., Hoang, A.T., Huang, N., Ortega, J., Scott, L.N., Chen, H.C., Patel, A.Y., Yakhshi-Tafti, R., Kim, K., and Hugo, W. (2023). Clonally expanded, thyrotoxic effector CD8 T cells driven by IL-21 contribute to checkpoint inhibitor thyroiditis. Sci. Transl. Med. *15*, eadg0675. https://doi.org/10.1126/scitranslmed.adg0675.
9. Munir, A.Z., Gutierrez, A., Qin, J., Lichtman, A.H., and Moslehi, J.J. (2024). Immune-checkpoint inhibitor-mediated myocarditis: CTLA4, PD1 and LAG3 in the heart. Nat. Rev. Cancer *24*, 540–553. https://doi.org/10.1038/s41568-024-00715-5.
10. Zhu, H., Galdos, F.X., Lee, D., Waliany, S., Huang, Y.V., Ryan, J., Dang, K., Neal, J.W., Wakelee, H.A., Reddy, S.A., et al. (2022). Identification of Pathogenic Immune Cell Subsets Associated With Checkpoint Inhibitor-Induced Myocarditis. Circulation *146*, 316–335. https://doi.org/10.1161/circulationaha.121.056730.
11. Perret, R.E., Josselin, N., Knol, A.C., Khammari, A., Cassecuel, J., Peuvrel, L., and Dreno, B.; Supported by GESTIM Nantes group of cutaneous adverse events induced by anticancer drugs (2017). Histopathological aspects of cutaneous erythematous-papular eruptions induced by immune checkpoint inhibitors for the treatment of metastatic melanoma. Int. J. Dermatol. *56*, 527–533. https://doi.org/10.1111/ijd.13540.
12. Farina, A., Villagrán-García, M., Vogrig, A., Zekeridou, A., Muñiz-Castrillo, S., Velasco, R., Guidon, A.C., Joubert, B., and Honnorat, J. (2024). Neurological adverse events of immune checkpoint inhibitors and the development of paraneoplastic neurological syndromes. Lancet Neurol. *23*, 81–94. https://doi.org/10.1016/s1474-4422(23)00369-1.
13. Ma, Y., Zeng, J., Ding, F., Xu, Y., Wang, Y., Zhong, G., Liu, N., Wang, Y., Li, Y., Chen, S., et al. (2024). Cerebral F-FDG PET/CT Metabolism as Diagnostic Signature for Central Nervous System Toxicity After Immune Checkpoint Blockade Cancer Treatment. J. Nucl. Med. *65*, 1129–1136. https://doi.org/10.2967/jnumed.123.267025.
14. Müller-Jensen, L., Schulz, A.R., Mei, H.E., Mohr, R., Ulrich, C., Knape, P., Frost, N., Frischbutter, S., Kunkel, D., Schinke, C., et al. (2024). Immune signatures of checkpoint inhibitor-induced autoimmunity-A focus on neurotoxicity. Neuro Oncol. *26*, 279–294. https://doi.org/10.1093/neuonc/noad198.
15. Yasuda, Y., Iwama, S., Sugiyama, D., Okuji, T., Kobayashi, T., Ito, M., Okada, N., Enomoto, A., Ito, S., Yan, Y., et al. (2021). CD4 T cells are essential for the development of destructive thyroiditis induced by anti-PD-1 antibody in thyroglobulin-immunized mice. Sci. Transl. Med. *13*, eabb7495. https://doi.org/10.1126/scitranslmed.abb7495.
16. Tadokoro, T., Keshino, E., Makiyama, A., Sasaguri, T., Ohshima, K., Katano, H., and Mohri, M. (2016). Acute Lymphocytic Myocarditis With Anti-PD-1 Antibody Nivolumab. Circ. Heart Fail. *9*, e003514. https://doi.org/10.1161/circheartfailure.116.003514.
17. Sasson, S.C., Slevin, S.M., Cheung, V.T.F., Nassiri, I., Olsson-Brown, A., Fryer, E., Ferreira, R.C., Trzupek, D., Gupta, T., Al-Hillawi, L., et al. (2021). Interferon-Gamma-Producing CD8 Tissue Resident Memory T Cells Are a Targetable Hallmark of Immune Checkpoint Inhibitor-Colitis. Gastroenterology *161*, 1229–1244.e9. https://doi.org/10.1053/j.gastro.2021.06.025.
18. Zen, Y., and Yeh, M.M. (2019). Checkpoint inhibitor-induced liver injury: A novel form of liver disease emerging in the era of cancer immunotherapy. Semin. Diagn. Pathol. *36*, 434–440. https://doi.org/10.1053/j.semdp.2019.07.009.
19. Marini, A., Bernardini, A., Gigli, G.L., Valente, M., Muñiz-Castrillo, S., Honnorat, J., and Vogrig, A. (2021). Neurologic Adverse Events of Immune Checkpoint Inhibitors: A Systematic Review. Neurology *96*, 754–766. https://doi.org/10.1212/wnl.0000000000011795.
20. Ma, Y., Liu, N., Wang, Y., Zhang, A., Zhu, Z., Zhang, Z., Li, Y., Jian, G., Fu, G., Dong, M., et al. (2023). Cognitive adverse events in patients with lung cancer treated with checkpoint inhibitor monotherapy: a propensity score-matched analysis. eClinicalMedicine *59*, 101987. https://doi.org/10.1016/j.eclinm.2023.101987.
21. Graus, F., and Dalmau, J. (2019). Paraneoplastic neurological syndromes in the era of immune-checkpoint inhibitors. Nat. Rev. Clin. Oncol. *16*, 535–548. https://doi.org/10.1038/s41571-019-0194-4.

22. Farina, A., Villagrán-García, M., Ciano-Petersen, N.L., Vogrig, A., Muñiz-Castrillo, S., Taillandier, L., Michaud, M., Lefilliatre, M., Wang, A., Lepine, Z., et al. (2023). Anti-Hu Antibodies in Patients With Neurologic Side Effects of Immune Checkpoint Inhibitors. Neurol. Neuroimmunol. Neuroinflamm. *10*, e200058. https://doi.org/10.1212/nxi.0000000000200058.

23. Müller-Jensen, L., Knauss, S., Ginesta Roque, L., Schinke, C., Maierhof, S.K., Bartels, F., Finke, C., Rentzsch, K., Ulrich, C., Mohr, R., and Stenzel, W. (2023). Autoantibody profiles in patients with immune checkpoint inhibitor-induced neurological immune related adverse events. Front. Immunol. *14*, 1108116. https://doi.org/10.3389/fimmu.2023.1108116.

24. Bartels, F., Strönisch, T., Farmer, K., Rentzsch, K., Kiecker, F., and Finke, C. (2019). Neuronal autoantibodies associated with cognitive impairment in melanoma patients. Ann. Oncol *30*, 823–829. https://doi.org/10.1093/annonc/mdz083.

25. Hirota, K., Hashimoto, M., Yoshitomi, H., Tanaka, S., Nomura, T., Yamaguchi, T., Iwakura, Y., Sakaguchi, N., and Sakaguchi, S. (2007). T cell self-reactivity forms a cytokine milieu for spontaneous development of IL-17+ Th cells that cause autoimmune arthritis. J. Exp. Med. *204*, 41–47. https://doi.org/10.1084/jem.20062259.

26. Beringer, A., and Miossec, P. (2019). Systemic effects of IL-17 in inflammatory arthritis. Nat. Rev. Rheumatol. *15*, 491–501. https://doi.org/10.1038/s41584-019-0243-5.

27. Gardin, T., and Longbrake, E.E. (2021). The Role of Immune Checkpoint Therapy in Propagating Neurologic Immune-Related Adverse Events: Inducing or "Unmasking" Autoimmunity? Neurology *96*, 733–734. https://doi.org/10.1212/wnl.0000000000011812.

28. Sechi, E., Markovic, S.N., McKeon, A., Dubey, D., Liewluck, T., Lennon, V.A., Lopez-Chiriboga, A.S., Klein, C.J., Mauermann, M., Pittock, S.J., et al. (2020). Neurologic autoimmunity and immune checkpoint inhibitors: Autoantibody profiles and outcomes. Neurology *95*, e2442–e2452. https://doi.org/10.1212/wnl.0000000000010632.

29. Schober, K., Voit, F., Grassmann, S., Müller, T.R., Eggert, J., Jarosch, S., Weißbrich, B., Hoffmann, P., Borkner, L., Nio, E., et al. (2020). Reverse TCR repertoire evolution toward dominant low-affinity clones during chronic CMV infection. Nat. Immunol. *21*, 434–441. https://doi.org/10.1038/s41590-020-0628-2.

30. Seki, M., Kitano, S., and Suzuki, S. (2022). Neurological disorders associated with immune checkpoint inhibitors: an association with autoantibodies. Cancer Immunol. Immunother. *71*, 769–775. https://doi.org/10.1007/s00262-021-03053-9.

31. Räuber, S., Schroeter, C.B., Strippel, C., Nelke, C., Ruland, T., Dik, A., Golombeck, K.S., Regner-Nelke, L., Paunovic, M., Esser, D., and Muench, C. (2023). Cerebrospinal fluid proteomics indicates immune dysregulation and neuronal dysfunction in antibody associated autoimmune encephalitis. J. Autoimmun. *135*, 102985. https://doi.org/10.1016/j.jaut.2022.102985.

32. Das Sarma, J., Ciric, B., Marek, R., Sadhukhan, S., Caruso, M.L., Shafagh, J., Fitzgerald, D.C., Shindler, K.S., and Rostami, A. (2009). Functional interleukin-17 receptor A is expressed in central nervous system glia and upregulated in experimental autoimmune encephalomyelitis. J. Neuroinflammation *6*, 14. https://doi.org/10.1186/1742-2094-6-14.

33. Ankathatti Munegowda, M., Deng, Y., Chibbar, R., Xu, Q., Freywald, A., Mulligan, S.J., van Drunen Littel-van den Hurk, S., Sun, D., Xiong, S., and Xiang, J. (2011). A distinct role of CD4+ Th17- and Th17-stimulated CD8+ CTL in the pathogenesis of type 1 diabetes and experimental autoimmune encephalomyelitis. J. Clin. Immunol. *31*, 811–826. https://doi.org/10.1007/s10875-011-9549-z.

34. Kebir, H., Ifergan, I., Alvarez, J.I., Bernard, M., Poirier, J., Arbour, N., Duquette, P., and Prat, A. (2009). Preferential recruitment of interferon-gamma-expressing TH17 cells in multiple sclerosis. Ann. Neurol. *66*, 3. https://doi.org/10.1002/ana.21748.

35. Jacques, N., Marlieke, L.M., Jongsma, P., and Oddmund, B. (2011). Towards a systems understanding of MHC class I and MHC class II antigen presentation. Nat. Rev. Immunol. *11*, 12. https://doi.org/10.1038/nri3084.

36. Blaha, D.T., Anderson, S.D., Yoakum, D.M., Hager, M.V., Zha, Y., Gajewski, T.F., and Kranz, D.M. (2019). High-Throughput Stability Screening of Neoantigen/HLA Complexes Improves Immunogenicity Predictions. Cancer Immunol. Res. *7*, 50–61. https://doi.org/10.1158/2326-6066.cir-18-0395.

37. Munck, M., Berdini, V., Bevan, L., Brothwood, J.L., Castro, J., Courtin, A., East, C., Ferraldeschi, R., Heightman, T.D., Hindley, C.J., et al. (2021). ASTX029, a Novel Dual-mechanism ERK Inhibitor, Modulates Both the Phosphorylation and Catalytic Activity of ERK. Mol Cancer Ther. *20*, 1757–1768. https://doi.org/10.1158/1535-7163.MCT-20-0909.

38. Graus, F., Titulaer, M.J., Balu, R., Benseler, S., Bien, C.G., Cellucci, T., Cortese, I., Dale, R.C., Gelfand, J.M., Geschwind, M., et al. (2016). A clinical approach to diagnosis of autoimmune encephalitis. Lancet Neurol. *15*, 391–404. https://doi.org/10.1016/S1474-4422(15)00401-9.

39. Guidon, A.C., Burton, L.B., Chwalisz, B.K., Hillis, J., Schaller, T.H., Amato, A.A., Betof Warner, A., Brastianos, P.K., Cho, T.A., Clardy, S.L., et al. (2021). Consensus disease definitions for neurologic immune-related adverse events of immune checkpoint inhibitors. J. Immunother. Cancer *9*, e002890. https://doi.org/10.1136/jitc-2021-002890.

40. Cuzzubbo, S., Tetu, P., Guegan, S., Ursu, R., Belin, C., Villaros, L.S., Mazoyer, J., Lheure, C., Lebbe, C., Baroudjian, B., et al. (2020). Reintroduction of immune-checkpoint inhibitors after immune-related meningitis: a case series of melanoma patients. J. Immunother. Cancer *8*, 2. https://doi.org/10.1136/jitc-2020-001034.

41. Tzourio-Mazoyer, N., Landeau, B., Papathanassiou, D., Crivello, F., Etard, O., Delcroix, N., Mazoyer, B., and Joliot, M. (2002). Automated anatomical labeling of activations in SPM using a macroscopic anatomical parcellation of the MNI MRI single-subject brain. Neuroimage *15*, 273–289. https://doi.org/10.1006/nimg.2001.0978.

42. Wefel, J.S., Vardy, J., Ahles, T., and Schagen, S.B. (2011). International Cognition and Cancer Task Force recommendations to harmonise studies of cognitive function in patients with cancer. Lancet Oncol. *12*, 703–708. https://doi.org/10.1016/s1470-2045(10)70294-1.

43. Lange, M., Joly, F., Vardy, J., Ahles, T., Dubois, M., Tron, L., Winocur, G., De Ruiter, M.B., and Castel, H. (2019). Cancer-related cognitive impairment: an update on state of the art, detection, and management strategies in cancer survivors. Ann. Oncol. *30*, 1925–1940. https://doi.org/10.1093/annonc/mdz410.

44. Lim, J.A., Lee, S.T., Moon, J., Jun, J.S., Kim, T.J., Shin, Y.W., Abdullah, S., Byun, J.I., Sunwoo, J.S., Kim, K.T., et al. (2019). Development of the clinical assessment scale in autoimmune encephalitis. Ann. Neurol. *85*, 352–358. https://doi.org/10.1002/ana.25421.

45. Li, M., Hou, X., Zheng, L., Ma, Y., Li, D., Lv, Y., Chen, J., Zheng, W., Shao, Y., Mou, Y., and Chen, L. (2022). Utilizing phenotypic characteristics of metastatic brain tumors to improve the probability of detecting circulating tumor DNA from cerebrospinal fluid in non-small-cell lung cancer patients: development and validation of a prediction model in a prospective cohort study. ESMO Open *7*, 100305. https://doi.org/10.1016/j.esmoop.2021.100305.

46. Nilsson, J.B., Kaabinejadian, S., Yari, H., Kester, M.G.D., van Balen, P., Hildebrand, W.H., and Nielsen, M. (2023). Accurate prediction of HLA class II antigen presentation across all loci using tailored data acquisition and refined machine learning. Sci. Adv. *9*, eadj6367. https://doi.org/10.1126/sciadv.adj6367.

47. Muñiz-Castrillo, S., and Honnorat, J. (2024). Genetic predisposition to autoimmune encephalitis and paraneoplastic neurological syndromes. Curr. Opin. Neurol. *37*, 329–337. https://doi.org/10.1097/wco.0000000000001263.

48. Ramanathan, S., Brilot, F., Irani, S.R., and Dale, R.C. (2023). Origins and immunopathogenesis of autoimmune central nervous system disorders.

Nat. Rev. Neurol. *19*, 172–190. https://doi.org/10.1038/s41582-023-00776-4.

49. Bentzen, A.K., Marquard, A.M., Lyngaa, R., Saini, S.K., Ramskov, S., Donia, M., Such, L., Furness, A.J.S., McGranahan, N., Rosenthal, R., et al. (2016). Large-scale detection of antigen-specific T cells using peptide-MHC-I multimers labeled with DNA barcodes. Nat. Biotechnol. *34*, 1037–1045. https://doi.org/10.1038/nbt.3662.

50. Lyu, F., Han, F., Ge, C., Mao, W., Chen, L., Hu, H., Chen, G., Lang, Q., and Fang, C. (2023). OmicStudio: A composable bioinformatics cloud platform with real-time feedback that can generate high-quality graphs for publication. iMeta *2*, e85. https://doi.org/10.1002/imt2.85.

51. Austin, P.C. (2009). Balance diagnostics for comparing the distribution of baseline covariates between treatment groups in propensity-score matched samples. Stat. Med. *28*, 3083–3107. https://doi.org/10.1002/sim.3697.

52. Ziegel, E. (2004). Statistical Methods for Rates and Proportions. In Technometrics (Taylor & Francis).

## STAR★METHODS

### KEY RESOURCES TABLE

| REAGENT or RESOURCE | SOURCE | IDENTIFIER |
|---|---|---|
| Antibodies | | |
| antiCD3-Spark Blue 550 (SK7) | BioLegend, Cat# 344852; RR1D: AB_2819985 | 344852, 100 Tests |
| antiCD4-BV750 (SK3) | BioLegend, Cat# 344643; RRID: AB_2734346 | 344643, 25 Tests |
| antiPD1-BB515 (EH12.1) | BD Biosciences, Cat# 564494; RRID: AB_2738827 | 564494, 50 Tests |
| antiCCR7-PE/Fire810 (G043H7) | BioLegend, Cat# 353244; RRID: AB_2617001 | 353244, 100 Tests |
| antiCD45RA-BV510 (HI100) | BD Biosciences, Cat# 563031; RRID: AB_2722499 | 563031, 50 Tests |
| anti-CD3 (OKT3) | ThermoFisher, Cat# 14-0037-82; RRID: AB_467057 | Cat # 14-0037-82, 100 μg |
| anti-CD28 | ThermoFisher, Cat# 740009M; RRID: AB_2942253 | Cat #740009M, 100 μg |
| Biological samples | | |
| Cerebrospinal fluid (CSF) samples from patients with irAE-CNS, CNSI, AME, and non-irAE-CNS conditions. | Shantou University Medical College Affiliated Cancer Hospital, Sun Yat-sen University Cancer Center, The First Affiliated Hospital of Zhengzhou University, Hainan Hospital of the PLA General Hospital | ST-ZLY-2020-716 |
| Chemicals, peptides, and recombinant proteins | | |
| Overlapping 15-mer peptide pool, human NMDAR1 | Immudex™ | Customized |
| Overlapping 15-mer peptide pool, human SOX1 | Immudex™ | Customized |
| Overlapping 15-mer peptide pool, human DPYSL5 | Immudex™ | Customized |
| Overlapping 15-mer peptide pool, human ELAVL4 | Immudex™ | Customized |
| Overlapping 15-mer peptide pool, human GRIA1 | Immudex™ | Customized |
| Recombinant human IL-2 | Novoprotein™ | CYT-209 AmyJet scientific |
| APC-labeled dextran backbones | Klickmer™ | Customized |
| MHC II monomers with UV-sensitive ligands | Klickmer™ | Customized |
| Critical commercial assays | | |
| OLINK Inflammation Targeted Panel (406 proteins) | Olink | Inflammation-EXPLORE & Inflammation-TARGET |
| BD Rhapsody Single-Cell Multiomics System | BD Biosciences | N/A |
| BD Rhapsody Targeted mRNA and AbSeq Amplification Kit | BD Biosciences | 633801 |
| BD Rhapsody Immune Response Panel HS | BD Biosciences | 633750 |
| IsoCode Chip +32-Plex Antibody Barcode Chip | Bruker Cellular Analysis | ISOCODE-1001-4 |
| TNFRSF9 ELISA Kit | Sigma | RAB0554 |
| GZMB ELISA Kit | Sigma | RAB1498 |
| CCL11 ELISA Kit | Sigma | RAB0042 |

(*Continued on next page*)

*Continued*

| REAGENT or RESOURCE | SOURCE | IDENTIFIER |
|---|---|---|
| IL-17A ELISA Kit | Sigma | 03-0159-00 |
| MCP-4 ELISA Kit | Sigma | RAB0045 |
| MCP-1 ELISA Kit | Sigma | RAB1498 |
| Deposited data | | |
| Single-cell RNA sequencing data | This study | Genome Sequence Archive for Human, HRA016812 |
| Proteomics data | This study | PRoteomics IDEntifications Database (PRIDE), PAD000030 |
| Experimental models: Cell lines | | |
| SH-SY5Y | Boster Biological | CatNo.CX0092 |
| Software and algorithms | | |
| R software | R Project | 4.3.3 |
| Seurat | Satija Lab/NY Genome Center | 5.2.1 |
| OmicStudio | Shanghai Luming Biotechnology Co., Ltd. | https://www.omicstudio.cn/tool |
| Scenium | Siemens Healthineers | selenium 4.17 |
| FlowJo | BD Biosciences | 10.4.2 |
| Fiji (ImageJ) | Open Source Community | http://fiji.sc |
| GraphPad Prism | GraphPad Software | 8.0 |

## EXPERIMENTAL MODEL AND STUDY PARTICIPANT DETAILS

### Human subjects and clinical cohorts

This multicenter cohort study was approved by the Institutional Review Board of the Affiliated Cancer Hospital of Shantou University Medical College (Approval No. ST-ZLY-2020-716). All procedures were performed in accordance with the Helsinki Declaration. Written informed consent was obtained from all participants.

### Four independent clinical cohorts were enrolled

1. Cohort 1 (Discovery Cohort): Patients from the Affiliated Cancer Hospital of Shantou University Medical College and Second Affiliated Hospital of Shantou University Medical College (Dec 2019 – Jul 2020). Included irAE-CNS patients at onset (n = 30 for proteomics, n = 8 for single-cell analysis) and control groups [non-irAE-CNS (NC, n = 24), central nervous system infection (CNSI, n = 24), autoimmune paraneoplastic encephalopathy (AME, n = 35)].
2. Cohort 2 (Longitudinal Validation Cohort): Patients from Sun Yat-Sen Cancer Center and Cancer Hospital of Shantou University Medical College (Nov 2021 – Mar 2022). Included irAE-CNS patients (n = 20) for longitudinal sampling (onset, 5-month, 12-month) and control groups (NC, n = 9; CNSI, n = 16; AME, n = 13).
3. Cohort 3 (Antigen-Specific Validation Cohort): Patients from Cancer Hospital of Shantou University Medical College, First Affiliated Hospital of Zhengzhou University, and Hainan Hospital of PLA General Hospital (Aug 2022 – May 2023). Included irAE-CNS patients (n = 38) for NMDAR1-specific cell analysis.
4. Cohort 4 (Therapeutic Intervention Cohort): An observational, multi-center, match-controlled real-world cohort from Affiliated Cancer Hospital of Shantou University Medical College, Sun Yat-Sen Cancer Center, and Hainan Hospital of PLA General Hospital (Feb 2021 – Jan 2024). Included irAE-CNS patients treated with anti-IL-17A agents (n = 17) and propensity-score matched controls receiving standard care (n = 17).

### Summary of participant demographics

The age and gender distribution for all participants across the four cohorts are summarized in Table S7. Briefly, the median/mean age of irAE-CNS patients across cohorts ranged from 57 to 68 years, with a male predominance observed in most groups. Detailed demographic and clinical characteristics for each cohort are provided in Tables S1–S6.

### Diagnostic criteria for irAE-CNS and control groups

1. Diagnosis followed the Consensus Statement for Neurologic Immune-Related Adverse Events (Munck et al.[37]) and Graus et al. criteria for autoimmune encephalitis (Graus et al.[38]).
2. irAE-CNS: New-onset encephalitis, meningitis, demyelination, or cerebral vasculitis following Immune Checkpoint Inhibitor (ICI) initiation in cancer patients. Specific sub-type definitions (Meningitis, Encephalitis, Demyelinating encephalopathy,

CNS vasculitis) are provided in the main manuscript Methods section.
3. Autoimmune Paraneoplastic Encephalopathy (AME): Defined as paraneoplastic autoimmune encephalopathy in cancer patients without current or prior history of immunotherapy.
4. Central Nervous System Infection (CNSI): Diagnosed based on clinical presentation, CSF findings (pleocytosis, elevated protein), and microbiological/PCR testing.
5. Non-irAE-CNS Controls (NC): ICI-treated cancer patients without diagnosis of irAE-CNS or other active neurological conditions.

### Key exclusion criteria for all participants included

(1) Metastatic or thrombotic brain lesions interfering with imaging analysis; (2) Failed quality control for imaging or CSF specimen; (3) Active viral/bacterial infection, brain metastasis, or severe brain injury at recruitment/during follow-up; (4) History of brain radiotherapy; (5) Unreadable 18F-FDG PET/CT images due to artifacts.

### Experimental model: Cell line

The human neuroblastoma cell line SH-SY5Y was used for *in vitro* cytotoxicity assays. The cell line was obtained from Boster Biological and was tested negative for mycoplasma contamination. Cell line authentication was performed by the provider via short tandem repeat (STR) profiling.

## METHOD DETAILS

### Study design and cohort description

We conducted a multicenter, cohort study to explore the intracranial inflammatory environment in patients with immune-related adverse events affecting the central nervous system (irAE-CNS). The study involved four independent cohorts, with serial sampling of imaging data, clinical testing, and cerebrospinal fluid (CSF) analysis. Cohort 1 include patients from the Affiliated Cancer Hospital of Shantou University Medical College and Second Affiliated Hospital of Shantou University Medical College, enrolled between December 2019 and July 2020. Cohort 2 comprised patients from Sun Yat-Sen Cancer Center and Cancer Hospital of Shantou University Medical College, recruited from November 2021 to March 2022. Cohort 3 consisted of patients at Cancer Hospital of Shantou University Medical College, First Affiliated Hospital of Zhengzhou University and Hainan Hospital of PLA General Hospital enrolled between August 2022 and May 2023. Cohort 4 included patients at Affiliated Cancer Hospital of Shantou University Medical College, Sun Yat-Sen Cancer Center, and Hainan Hospital of PLA General Hospital, recruited from February 2021 to January 2024. Human participant study followed Institutional Review Boards at Cancer Hospital of Shantou University Medical College with approved protocols and required informed consent by all participants of the study. All sampling procedures were performed according to the Helsinki Declaration. Information related to demographic variables and treatment history of participants were obtained from electronic medical records at each research setting in which all participant data were de-identified. Cohort Reporting adhered to Strengthening the Reporting of Observational Studies in Epidemiology (STROBE) checklist for cohort studies.

Brain inflammation was assessed by radiologists via 18-F FDG PET/CT or MRI. The diagnosis of irAE-CNS onset or its exclusion was determined through consultations between neurologists and oncologists, with all clinical signs evaluated according to Common Terminology Criteria for Adverse Events (CTCAE, version 5.0). The date of irAE-CNS diagnosis was established by reviewing outpatient and inpatient medical records. Key exclusion criteria included 1) Metastatic or thrombotic brain lesions that interfered with imaging analysis; 2) Imaging or CSF specimen that failed quality control for analysis; 3) Active viral or bacterial infection, brain metastasis, or severe brain injury at recruitment or during follow-up; and 4) A history of Brain radiotherapy; 5) 18-F FDG PET/CT images deemed unreadable due to imaging artifacts or improper patient positioning during scanning.

The formal diagnosis of irAE-CNS was confirmed by at least two independent oncologists at the research sites who were not involved in this study. In addition to collecting CSF samples from ICI-treated cancer patients without an irAE-CNS diagnosis, we also include samples from patients with autoimmune paraneoplastic encephalopathy (AME) or central nervous system infection (CNSI). AME was defined as paraneoplastic autoimmune encephalopathy happening in cancer patients without current or history of immunotheray (including ICI). Pathology of AME was suggested to mimic irAE-CNS, both of which shared autoimmune backgrounds, although demographics and epidemiology are different.[21] AME and CNSI were diagnosed with criteria suggested by Graus et al.[38]

### Diagnostic criteria of irAE-CNS

irAE-CNS is defined as intracranial inflammatory adverse events following ICI treatment in cancer patients, involving meninges and parenchyma, with or without optic tract involvement. Diagnostic criteria of irAE-CNS followed Consensus Statement of Neurologic Adverse Events.[39,40] Briefly, irAE-CNS was defined as new-onset encephalitis, meningitis, demyelination, and intracerebral vasculitis following ICI initiation in cancer patients. irAE-CNS is referred here as any form of intracranial immune-related adverse events involving meninges, parenchyma, and optic tracts, defined in the Consensus Statement.[39,40] Specifically, the study included the following specified subtypes.

***Meningitis***

1. Clinical characteristics concord with meningitis, including meningitis triad (headaches, stiff neck, and nausea/vomiting), patient may present with photophobia. Excluding symptoms were: focal deficits, partial/complete seizures, or brain diseases suggesting parenchymal pathology.
2. Cerebral spinal fluid laboratory findings: pleocytosis (>5 WBC or >6 lymphocytes and/or protein >0.45 g/L, no tumor cells) without bacteria, streptococcal, or viral antigens. PCR of HSV is sometimes needed in susceptible individuals.
3. If MRI findings suggest patchy enhancement, additional lumbar punctures may be required to exclude carcinomatosis.

***Encephalitis***

1. Clinical characteristics follow encephalitis diagnosis, such as focal deficits and seizures.
2. Typical lesions, such as possible multifocal lesions, may raise suspicion of metastasis and should be excluded.
   a. T2-FLAIR hyperintensity and/or contrast enhancement on MRI brain scans (suggesting parenchymal abnormality);
   b. Inflammation on CSF studies (>5 WBC and/or elevated protein, no tumor cells), potentially with oligoclonal bands or increased IgG on CSF findings;
   c. Localizing EEG findings;
   d. Neuron-specific autoantibodies in serum and/or CSF consistent with autoimmune or para-neoplastic diseases.

***Demyelinating encephalopathy***

1. Clinical characteristics follow demyelinating encephalopathy, including acute optic neuritis, and transverse myelitis.
2. Serologic testing involves antibodies to aquaporin 4 and/or myelin oligodendrocyte glycoprotein.
3. Inflammation on CSF studies (pleocytosis, >5WBC, and/or elevated protein, no tumor cells).
4. Abnormal evoked potentials, and abnormal ophthalmic visual field testing in cases of optic neuritis.
5. MRI findings consistent with anatomical structures of relevant characteristics, such as optic neuritis.

***CNS vasculitis***

1. Symptoms and signs consistent with CNS vasculitis AND
2. Cerebral infarct, especially multiple CNS infarcts crossing vascular territories and no evidence for alternative cause such as thromboembolic disease.
3. Optional checkups: CNS vascular imaging (MRA, CTA or conventional angiogram) demonstrating vasculopathy consistent with vasculitis (e.g., vessel narrowing or beading).

### Sampling in longitudinal cohorts

Serial sampling was conducted by independent clinical coordinating technicians during follow-up in patients diagnosed with irAE-CNS. Sampling included 18-F FDG PET/CT, BFTs, and CSF specimen analysis across independent cohorts. Patients enrolled for study were followed up by experienced neurologists and oncologists in outpatient and inpatient setting during routine medical check-ups every 2–5 months at cancer check-up clinics of research site. 18-F FDG PET/CT and BFTs were used as clinical tools to evaluate disease progression of irAE-CNS after onset.[13] Follow-up sampling rationale was designed to co-occur with medical check-ups of irAE-CNS progression. Besides 18-F FDG PET/CT and BFT testing, all irAE-CNS patients received at least one acupuncture during follow-up to assess levels of intracranial inflammation. Lumbar puncture samples were procured after careful checkup of overall function, including locomotor and cancer-related assessment. Side effects of lumbar puncture and any accompanying adverse events were medically managed in research-site oncology inpatient clinic. In this study, CSF samples were obtained from all patients as discarded samples in neurological lab settings.

### 18F-FDG PET/CT scanning and image analysis

18F-FDG PET/CT brain imaging methods and image segmentation protocols have been previously published.[13] Briefly, patients fasted for >6 h prior to PET/CT scanning, performed with an integrated PET/CT scanners (Discovery ST 16, GE Healthcare), with parameters (3 min/bed position, matrix 200*200, field of view, or FOV, 740mm, slice thickness 3mm, and full width at half maxima, or FWHM, was 5 mm.). Head-to-thigh PET/CT scanning was performed for 45–60 min after 5 MBq/kg 18F-FDG injection and reconstruction was performed with ordered subset expectation maximization iterative algorithm. 18-F FDG PET/CT images were obtained in arms-down position to image head and neck area and in arms-up position in patients with no head and neck pathology to avoid artifacts. Brain imaging were obtained in arms-down positions across all cohorts. 18-F FDG PET/CT images with unreadable artifacts or altered positioning would be excluded.

OSEM PET/CT images were automatically segmented into brain lobes using Scenium software (Siemens Healthcare) which had been previously reported.[13] Built-in brain templates within Scenium that contained 3D structures fitting regions were adopted and thus uptake values of each cortical and sub-cortical regions were calculated as mean standard uptake value (SUVmean).The SUV was normalized based on weight and injected dose, the formula is provided in Figure S2.

The template automatically segmented regions of interest with license from CEA/Groupe d'Imagerie Fonctionnelle according to automated anatomical labeling (AAL) standards.[41] In the current study, we monitored SUVmean values of the following brain regions bilaterally: temporal lobe (TEM), cerebellum (CER), frontal lobe (FRONT), occipital lobe (OCC), parietal lobe (PAR), limbic area (LIM), brain stem (STEM), and whole brain (WB).

### Brain function tests

At each timepoint, irAE-CNS patients were evaluated with neurologists using clinician-rated scales and objective cognitive tests to evaluate brain functional status, which was collectively named as brain function tests (BFTs). BFTs were designed to monitor overall patient functions and pivotal levels of cognitive functions in patients with brain pathologies.[42] These tests, taken together, were suggested in prior research as consistent to multi-level prognosis of brain pathologies during mid-to-long term follow-up.[42,43] Illustrations of BFTs were shown in Table S6. They included 4 results from three tests. Modified Rankin Scale (mRS) aimed to evaluate overall functional status related to neurological diseases. Clinical Assessment Scale in Autoimmune Encephalitis (CASE) is a clinician-assessed scale covering overall functions of autoimmune-related CNS diseases, with relatively high level of consistency in assessing autoimmune brain pathologies.[44] Hopkins Verbal Learning Test-Revised (HVLT, divided into two segments HVLTi and HVLTd) are objective psycho-cognitive tests to specifically assess short-and long-term memory status.

### CSF proteomic assay

CSF sample processing has been previously reported, in which CSF specimen were centrifugated at 4°C, 1900g for 10 min (to collect cells of the CSF).[45] The supernatant were centrifugated again at 16 000g for 10 min. The supernatant was then stored at −80°C for further analysis. Proteins were measured using the Proximity Extension Assay (PEA, Olink tailored panel) according to the manufacturer's instructions. Briefly, oligonucleotide-labeled antibody probe pairs conjugated to targeted protein. Should probe pairs illustrate close proximity, oligonucleotides would hybridize in pairwise fashion. Addition of DNA polymerase leads to proximity-dependent polymerization event, generating specific PCR sequences. DNA sequence is subsequently quantified with microfluidic real-time PCR. Data were quality controlled and normalized with extension control and inter-plate control, to adjust for intra- and inter-run variation. The final readout was presented as Normalized Protein eXpression (NPX) values, which was arbitrary unit from 0 to 100 from a normalized and log-transformed scale, where high value corresponding to higher protein expression. Assay validation data are available on manufacturer's website (www.olink.com).

### Single-cell secreting proteomics

Cells from fresh (<1h upon procurement) CSF were obtained with centrifugation at 4°C, 1900g for 10 min. Upon experiment, cells were loaded into 96 wells pre-coated with anti-CD3 (OKT3, ThermoFisher) and anti-CD28 (ThermoFisher) at the density of $1 \times 10^5$/200μl, and cultured in completed RPMI media (Fisher Scientific) plus 10 ng/mL IL-2 (Biolegend) at 37°C, 5% CO2 for 16h. Cells were then loaded onto an IsoCode Chip and incubated at 37°C, 5% CO2 for 16 h. Following this incubation, secreted proteins from 100 to 2000 cells/sample were captured by the 32-plex antibody barcoded chip and analyzed by backend fluorescence ELISA-based assay. Poly6+ cell was here defined as a cell that can co-secrete 6 proteins (IL-17, MCP1. MCP4, Granzyme B, CCL11 and CD137).

### Single-cell VDJ repertoire, membranous proteomic, and RNA sequencing

Single-cell libraries were constructed via BD Rhapsody Express system (BD Biosciences, #633707) according to the manufacturer protocol (BD Biosciences). Cells were labeled with cell-specific tag and donor-specific identification tag (BD Biosciences, #633781). Cells were then put onto stain buffer wash (BD Biosciences, #554656), followed by pooled incubation of Fc block and per-cell surface protein antibody labeling (BD AbSeq Ab-Oligos master mix). Cells were pooled to reach 1000-20,000 count in 600-700mL buffer fluid. Primed cartridges were applied to load pooled cells (incubated at room temperature) and then to load cell beads after washing. These were incubated and washed twice with sample buffer, and then cells were lysed. Reverse transcription was carried out after retrieval of beads and washing.

Subsequent steps were related to VDJ and membranous proteomic sequencing library protocol to generate libraries using BD Rhapsody system. During reverse transcription, Poly-T Template Switching Oligo was added to allow for finding VDJ recombination events. Nucleotides were denatured, hybridized and went through Klenow extension (New England Biolabs, #M0212L) and treatment with Exonuclease. CDNAs were prepared in nested PCR reaction, followed by index PCR with targeted mRNA, Amplification Kit (BD Rhapsody, #633774), and Immune Response Panel (BD Rhapsody, #633750). Library concentration was calculated with dsDNA Assay Kit (Qubit, ThermoFisher, #Q32851). Quality control was performed with TapeStation with High Sensitivity D5000 ScreenTape (Agilent 2200).

Sample tags, mRNA, and antibody barcode reads were trimmed to 75nt, and VDJ libraries trimmed to 225nt, followed by sequencing on a Novaseq SP flow at 75*225. Refined calling was disabled on analysis pipeline (BD Rhapsody, https://www.sevenbridges.com/bdgenomics/).

### Single-cell data analysis

Preprocessing and cluster analysis was performed with ''Seurat'' package on R Statistics. Cells without any feature and features with <50 cells were excluded from matrix. Dimension reduction was first performed by principal component analysis (PCA) and then by Uniform Manifold Approximation and Projection (UMAP) embeddings to see unsupervised clustering of single cells. PCA was carried out with all features for analysis. Elbow plot was adopted to identify significant components, and 4 components were applied for UMAP plot in each analysis, with resolution set as 0.1. Default-parameter ''FindAllMarkers'' function was adopted to mark specific cluster with 25% difference from all other clusters. For secreting and surfacing proteomics, global scaling was

performed prior to log-transformation and centering from counts of surface barcode sequencing or illuminant secreting index. Secondary filtering was performed on membranous proteomics to remove mitochondrial and ribosomal expression-related cells.

Single-cell VDJ files went through default-parameter Cellranger VDJ 4.0 pipeline to generate clonotype information. Reads were referred to and annotated by human reference in IGBLAST database of NCBI. Information was then manually entered into single-cell proteomic Seurat object as combined phenotype-clonotype matching in each cell with the help of cell barcodes. Clonotype was defined as combined information of VDJ sequences shared by all such cells. Cells with one same clonotype were defined as the same cell clone. Clonal expansion was defined as frequency of cells with one same clonotype. Dominant clonotypes were defined as those with >5% expanded per patient sample. Persistent clonotypes were defined as identical clonotypes shared between all sampling timepoint during follow-up. If any clonotype was find to be both dominant and persistent, these cells would be marked as persistently clonally expanded.

In antigen-reactive single-cell VDJ clonotype analysis, inflated clonotypes were defined as >5% expanded clonotypes in antigen-reactive cells. Specific clonotypes were defined as single peptide-bound clonotypes while unspecific ones were defined as those binding >1 peptides. These data allowed for association analysis between VDJ clonotypes and cell phenotype (membranous proteomics). Finally, cells with both chains of VDJ sequences passed quality control for analysis. As such, clonotypes were defined as paired VDJ sequences of both chains in TCRf$\alpha\beta$, TCR$\gamma\delta$, or BCR-heavy/light chains.

### Candidate peptide prediction and pMHC multimerization

We adopted online bio-informatic prediction procedure NetMHCIIpan (http://www.cbs.dtu.dk/services/), to find 15-mer MHCII epitopes in five proteins hypothesized previously to be associated with irAE-CNS.[21,46,47] Thirty-three HLA type II proteins most frequently expressed in autoimmune and other related pathologies were used to find candidate peptide during bio-informatic prediction.[47,48] A 15-mer peptide capable of binding to HLA molecules were predicted from amino acid chains constituting the 5 proteins. Predicted peptides with Rank scores of less than 1% were adopted here as final candidates.

The pMHC complexes were produced using UV-mediated conditional ligand exchange, a process which was published elsewhere and briefly stated here.[49] Initially, MHCII monomers carrying UV-sensitive ligands were combined with corresponding peptides, resulting in a final concentration of 50 μg/mL monomer and 100 mM peptide. Mixture was put to UV light exposure for 1 h. Subsequently, pMHC complexes were joined with barcode + APC-labeled dextran backbones to reach 35 μg/mL for monomer and 3.5 to 4 $\times$ $10^{-8}$ M for labeled dextran backbone, followed by 30-min ice-bound incubation. In this process a buffer was added (PBS +0.5% BSA +80 μg/mL herring DNA +2 mM EDTA +5% glycerol +1000 nM biotin). After an additional half-hour ice-bound incubation, pMHC multimers were stored at $-20^{\circ}$C.

As such we selected 415 15-mer candidate peptides from all 5 proteins. These HLA-binding peptides were synthesized into pMHC monomers by UV-induced exchange. Monomers were then multimerized onto APC-labeled polysaccharide backbone and coupled with DNA barcode specific to each specific pMHC. We then mixed these multimers to sort cells in CSF-derived samples of irAE-CNS donors to yield cells corresponding to candidate peptides (named as multimer+sorted cells).

### Flow cytometry staining and sorting

Cells (<1h from lumbar puncture) were stained with the following antibodies (30–40 min, 4°C) indicated for surface protein staining: antiCD3-Spark Blue 550 (SK7, BioLegend), antiCD4-BV750 (SK3, BioLegend), antiPD1-BB515 (EH12.1, BD), antiCCR7-PE/Fire810 (G043H7, BioLegend), antiCD45RA-BV510 (HI100, BD). Cells were then washed and acquired by a spectral flow cytometer (Cytek). The data were analyzed by FlowJo 10.4.2. Directly conjugated murine IgG1 and IgG2 was adopted as background stain. CD4 subsets were defined by the expression of CD45RA and CCR7: naive (CD45RA + CCR7+), effector memory expressing CD45RA (CD45RA + CCR7-), central memory (CD45RA-CCR7+) and effector memory (CD45RA-CCR7-). Four-laser BD FACSAria Fusion cell sorter was adopted to enrich poly6+ T cells (CD137+ $CD4^+$ T cells) with gating strategy and panel identical to flow cytometry analysis. Intact cells were gated via forward scatter and side scatter (FSC-A/SSC-A). Doublets were dropped via FSC-H/FSC-W followed with SSC-H/SSC-W gates. Cells were subsequently sorted via 70μM nozzle (70 psi) to reach >98% purity. In cellular experiments, cells were sorted into cold RPMI with 10% FBS. For antigen-specific T cell sorting and sequencing, labeled pMHC multimers were thawed, centrifuged for 3 min at 3000g, and 2 μl pMHC unique to each irAE-CNS donor was obtained from the top of well and pooled according to HLA type selected. Reagent pool volume was cautiously reduced by ultrafiltration to reach final pMHC volume of 90-100μL. Isolated CD137+ cells were stained with donor-specific candidate pMHC reagents on ice for 20 min. Human Fc receptor blocking agent (TruStain FcX, BioLegend) was adopted to avoid unspecific binding. Multimer+ cells were sorted into single cells with FACSAria III sorters (BD Biosciences).

### ELISA

Levels of all 6 proteins (TNFRSF9, GZMB, CCL11, IL17A, MCP4, MCP1) in culture supernatant were quantified using the ELISA kit (Sigma-Aldrich). All procedures were performed according to the manufacturer instructions. Absorbance at 450 nm was measured using a microplate spectrophotometer (Multiskan Sky 1530, Thermo Fisher Scientific, USA).

## QUANTIFICATION AND STATISTICAL ANALYSIS

Statistical analyses were conducted using R software (version 4.3.3), with data visualization performed using OmicStudio tools at https://www.omicstudio.cn/tool.[50] A two-sided *p*-value <0.05 defined statistical significance. For multiple comparisons, *p*-values were adjusted using the Benjamini-Hochberg procedure to control the false discovery rate (FDR). Continuous data are presented as mean ± standard error of the mean (SEM) or median with interquartile range (IQR), as appropriate. Categorical variables are reported as counts and proportions. Group comparisons for continuous variables utilized the Mann-Whitney U test or unpaired Student's *t* test following normality assessment with the Shapiro-Wilk test. Paired continuous data were analyzed with the Wilcoxon signed-rank test. Categorical variables were compared using Chi-square or Fisher's exact tests, with McNemar's test applied for paired categorical assessments.

In Cohort 4, propensity score matching (PSM) was employed to balance baseline characteristics. Propensity scores were derived from a multivariable logistic regression model that included age, gender, smoking status, body mass index, cancer stage, ECOG performance status, time from ICI initiation to irAE-CNS onset, and irAE-CNS subtype. Calculated scores of 2 comparable groups were 1:1 paired. Matching quality was evaluated with standardised mean difference, calculated for each variable in the logistic model.[51,52] Any variable match with SMD over ($\sqrt{}$ ((n1 +n2)/n1*n2))*1.96 is regarded as imbalanced matching (n1 and n2 stood for pre-matched sample sizes).[51] Differential expression analysis of proteomic data was performed using linear models from the limma R package. Differences in flow cytometry data were assessed using non-parametric tests (Mann-Whitney U or Kruskal-Wallis), with antigen-specific T cell frequencies determined against a threshold set at the 99th percentile of negative control signals. Given the rarity of irAE-CNS and the exploratory nature of this study, a formal sample size calculation was not performed; patient enrollment was sequential without randomization, and investigators were not blinded to group allocation during laboratory analyses. All clinical outcome assessments for Cohort 4 were conducted retrospectively.

In all figures, asterisks denote statistical significance as follows: $*p < 0.05$, $**p < 0.01$, $***p < 0.001$, $**p < 0.0001$. Exact *p*-values and the specific statistical tests used for each figure are described in the corresponding figure legends."